Int. J. Appl. Comput. Math (2022) 8:130
https://doi.org/10.1007/s40819-022-01316-2

ORIGINAL PAPER

ABC Fractional Order Vaccination Model for Covid-19 with Self-Protective Measures

G. M. Vijayalakshmi[1] · **P. Roselyn Besi**[2]

Accepted: 2 April 2022 / Published online: 12 May 2022

Abstract
A mathematical model delineating the control strategies in transference of Covid-19 pandemic is examined through Atangana–Baleanu Caputo type fractional derivatives. The total count of people under observation is classified into Susceptible, Vaccinated, Infected and Protected groups (SVIP). The designed model studies the efficiency of vaccination and personal precautions incorporated qualitatively by every individual via fixed point theorem. Stability of the system has been investigated with spectral characterisation of Ulam Hyer's kind. Numerical interpolation has been derived by Adam's semi-analytical technique and we have approximated the solution. We have proved the theoretical analysis through graphical simulations that vaccination and self protective interventions are the significant role to decrease the contagious expansion of the virus among the people in process.

Keywords Covid-19 pandemic · ABC derivatives · Multi control measures · Fixed point theorems · Stability of Hyer Ulam's kind · Adam's Bashforth interpolation

Introduction

Infectious diseases have resilient impacts on public health overseas. COVID-19 pandemic has provoked depletion in health and wealth of the human society since the day of its explosion in the market of Wuhan, China from December 2019. The entire world is facing the iterative mayhem arouse as its consequences at full throttle with 437,333,859 confirmed infective cases and 5,960,972 persons died due to the harshness of the viral disease [1]. Coronaviruses cause illness with common cold affecting the air way organ of human body. Symptoms of this vulnerable disease include breathing trouble, body ache, sore throat, runny nose, nausea, vomiting and diarrhoea [2, 3]. Delta virus, Omicron were few new mutations of nCov-19

✉ P. Roselyn Besi
besi.roselyn@gmail.com

G. M. Vijayalakshmi
vijidaya105@gmail.com

1 Department of Mathematics, Vel Tech Rangarajan Dr. Sagunthala R & D Institute of Science and Technology, Avadi, Tamilnadu 600062, India

2 PG and Research Department of Mathematics, Auxilium College, Vellore, Tamilnadu 632006, India

with nippy transmission and inclined fatalities [4]. The Government with health department have planned effective control strategies. Multiple control measures such as vaccination, self hygienic habits help in breaking the transference link in a faster note [5]. Knowing the severity of the virus is primary to implement control measures and notify to the heedless. 'An ounce of prevention is worth a pound of cure' recommend that personal precautionary measures is the major control strategy. Guarding unvaccinated family members, babies below 5 years of age, pregnant women, immune-compromised high risk individuals place top in the list [6]. Copious self curb measures such as covering mouth and nose with a mask, be isolated, neglecting crowds, personal hygiene, disinfecting hands and avoid touching eyes,ears, nose and mouth were forced to follow strictly. Non-pharmaceutical immunity boosters armed us to defend the dreadful virus naturally. Herbal nutraceutical diet with warm water intake, meditation, Pranayama practice, turmeric, cumin, coriander and garlic rich foods, steam inhalation, herbal tea improvises and regulates airway passage in process triggering the defence system onset. Mass inoculation on emergency mode is also an efficient control method during pandemic situation. Innoculation doses combats every individuals to defense the exposure of the viral contaminated neighbourhoods. Successful implementation of vaccine shots to each and every susceptible adults results in reducing the infectious complications of the disease [7, 8]. To face the hazardous stream of microparasitic invasion, several vaccines have been developed and totally seven were approved in India, out of which Covishield, Covaxin and Sputnik V were used for vaccination drive since Jan 2021, to downstream the morbidity and fatalities. In India, vaccination programmes were commenced initially to strengthen the national health care system by vaccinating health care professionals, workers and adult groups above 60 years of age from March 2021. Later, the vaccine shots were injected for other age groups above 18 years eventually. All Indians inspite of their economic status, were entitled to vaccination process at free of cost.Due to abundant precautionary actions against the emerging mutants of variants of concern (Voc), inoculating children of 15–18 years age, have been initiated from Jan 3, 2022 very effectively [9]. Covid-19 vaccines quicken up the immunity by supplying a sack of memory cells called T- Lymphocytes and B- Lymphocytes to arm from infections latterly [9, 10]. Indefiance of the high impactness of vaccines over the late virulent strains, vaccine efficacy wanes rapidly after 6 months of duration, urging the necessity of booster shots to protect the people from death and more complexity [10–12].

Mathematical modelling the real world complex phenomena help us to understand the dynamics of a problem. Recently, Epidemic modelling equations in terms of arbitrary order visualises the transference dynamics and control process of contagious diseases. Epidemiological models occupies an impulsive act in COVID-19 disease dynamics with improvised awareness on the basics of a specific illness. The dynamical behaviour of disease spread is well understood by modelling the phenomena. Despite this, mathematical models of wide usage in several microphysical phenomena covers Magnetohydrodynamics(MHD) of 2D, 3D fluid flow, nano fluid flows and thermal conduction. Physical dynamics of electrically conducting fields using homotopy analysis were studied in [13] by parameters influencing heat transfer and velocity through MHD electro-osmosis in non-Newtonian fluid with various viscosity used to design micro-biomedical chips and DNA study in [14], magnetic effect and radiative flow of Maxwell nanoliquid system depicts the gradual rising of thermal parameters resulting in reduced level of microorganisms, mixed convective entropy [15], Brownian motion and thermophoresis of MHD flow in Buongiorno model [16]. Nonlinear models of stretching and free stream velocities predicted heat generation/absorption and stagnation point flow at an inclined applied magnetic field and tangent hyperbolic material [17, 18], Cattaneo-Christov heat flux model comparing 2D squeezing flow with that of Fourier's law of heat conduction [19] and effects of nanofluid flow using Von Karman transformations [20].

Many modelling scientists have contributed several results involving systems of ordinary calculus which employs only the current state activities and also inaccurate about its real existing state. To its contrast, fractional order systems with non-local aspects globalise the past history covering a vast neighbourhood matters. The global functioning of fractional calculus attracts analysts to analyse real world anomalous issues of many fields. The transmission dynamics of an epidemic model demands for the memory patterns, past events and inbuilt hereditary of micropathogenic infections on host's immunity. To all intents and purposes arbitrary order calculus with long term memory is the most preferable tool by many researchers [21]. The neighbourhood covering feature of fractional kernels indulge a more sensible approach for simulating COVID-19 pandemic dynamics. In contempt of untiring computations of fractional operators, variety of numerical algorithms have been solved for rapid convergence of solutions. In addition to this, biophysical applications of fractional order models include Caputo modelling of Casson fluid with Fourier's law [22], digital mask control design using Atangana Baleanu derivatives were investigated by Ghanbari and Atangana effectively [23], disease dynamics of various biological models also been studied for visceral leishmaniasis [24], dengue fever therein [25] and toxoplasmosis investigated therein [26].

Fractional calculus formulates non-integer type integrals and derivatives [27]. Great Mathematicians Riemann–Liouville, Letnikov etc. have contributed their findings on singular exponential kernels, while Caputo–Fabrizio (CF) and Atangana–Baleanu (AB) developed non-singular Mittag–Leffler kernel operators [28]. Both CF and AB type integrals are extensively used by biologists, physicist and electro-chemical therapists [29–31]. The newlier preeminent definition captivated by Atangana, Baleanu and Caputo is ABC derivative in 2016, which exhibits singular kernel via non-singular kernel detailed in [28–38]. Some of the up-to date fractional models employing estrange kinetic energy were solved efficiently in fluid flow, diffusive behaviour analysis, Earthquake dynamics, viscoelasticity properties,damping oscillator and optical sciences, Astro and chemical physics, Finance, Geological changes etc..Fractional order models of some physical unsteady natural convection, Newtonian effect, MHD of Maxwell fluid in AB and CF forms using Laplace transformation and impact of magnetic effect on heat transfer over porous inclined surface were explored in [32, 33] Fractional derivatives and integrals are used for analysis of disease models effectively for its non-local behaviour. The memory index of the biological immune system have been deeply captured in in [34, 35]. Fractional order reproducing kernel algorithms were also developed and studied efficiently for physical interpretations of Lienard's equation and damping Van der pol oscillator by authors in [36, 37]. Numerical solutions for Fredholm and Volterra type integro differential equations were analysed and contributed by authors for fractional AB type derivatives as well in [38, 39]. The Mittag Leffler function is the multifaceted function in recent fractional order epidemiological systems which inherits the reproducing memory principle. Analytical herd behaviour of infected prey on predators influenced by external toxicants were studied in [40, 41].

India reported 38,566,027 positive infected cases with 488,422 deaths with 99% recovery rate as of February 2022. Various predictive models have been formulated on COVID-19 disease in recent days. Kamal Shah et al., framed a COVID-19 mathematical model and thoroughly analysed the effectual reactions of the disease [42]. Oud, M.A, Ali, et al., studied the disease model on COVID-19 with multicontrols quarantine and isolation [43]. Muhammed Sinan et al., have analysed a compartmental model PSEIT with control strategies inhibited more feasibly [44]. Qualitative and stability in Hyer Ulam's style [45] analysis of fractional Caputo type model have been demonstrated by several modelling analysts and the better desired result have been suggested for most minimal order of derivatives [42–48]. In this work, we present a novel epidemiological model of ABC derivatives for COVID-19 with

effective self-hygienic control. This paper analyses SVIP model with self- precautionary activities avoiding new infections, infection rate of susceptibles, relapse rate of vaccinated susceptibles after the implementation of effective vaccination programme for immunising against COVID-19 ailment.

An ABC type non-integer order disease model that encapsulates vaccination and self-hygienic control measures to reduce the complicate virulence of the infection is built in this paper. The significant features investigated here are.

(i) the emergency need of vaccination in minimising viral transmission,
(ii) effect of increasing vaccination rate and reduced contact rate in reducing severity of the virus and
(iii) personal hygienic habitual impacts on self- protection against the exposed infectives.

This manuscript synopsizes the following sections, basic necessary definitions and results of ABC fractional derivatives were presented in "Preliminary Definitions and Results" section, Model formulation in "Formulation of Mathematical Model SVIP" section, Qualitative analysis with some basic properties of the model and its stability in "Basic Properties of the Model" section, Numerical formulation and the interpreted graphical results were discussed in "Numerical Method and Results" and "Results and Discussion" sections.

Preliminary Definitions and Results

In this section, some basic necessary definitions and fundamental results needed for the analysis of our model were presented. The fractal fractional derivative of ABC type is the most powerful of all other fractional operators, which integrates the memory kernel called Mittag Leffler function is defined on Banach space to employ the existence of solution for the non-linear system modelled in (1).

Definition 2.1 Let F be defined on the space [0, T], $F' = (0, T) \subset$ R, [0, T] = (F, R) be functions with continuity. Define T: [0, 1] → R satisfies,

$\|(\mathcal{S}, \mathcal{V}, \mathcal{I}, P)\| = \max_{t\in[0,T]} \{\|\mathcal{S}(t) + \mathcal{V}(t) + \mathcal{I}(t) + P(t)\|\}$ where $\mathcal{S}, \mathcal{V}, \mathcal{I}, P \in$ [0, T].

The fractal fractional derivative of ABC is given by,

$$\text{ABC}\ \ D^{\eta}_{0+}\,\text{f(t)} = \frac{M(\eta)}{1-\eta}\int_0^t \frac{d}{dy}\text{f(y)}K_{\eta}\left(\frac{-\eta}{1-\eta}(t-y)^{\eta}\right)\text{dy} \tag{1}$$

where $M(\eta) = (1-\eta) + \frac{\eta}{\Gamma\eta}$ is the normalisation operator takes only real positive values satisfying $M(\eta) = 1$ for $\eta = 0$ and 1, $\eta \in$ [0, 1]. The main purpose of applying this type of multipliers assures maintaining balance in modelling complex problems while integrating over the non-integer order η.

Here K_{η}-memory kernel of Leffler category, generalisation of exponential function given by

$$K_{\eta}(\text{f}) = \sum_{k=0}^{\infty} \frac{f^k}{K\eta + 1} \tag{2}$$

The corresponding integral is defined as follows,

$$\text{AB } I_{f(t)} = \frac{1-\eta}{M(\eta)}\text{f(t)} + \frac{\eta}{M(\eta)\Gamma\eta}\int_0^t (t-y)^{\eta-1}\text{f(y)}\,\text{dy} \tag{3}$$

The first term exists in (4) for $\eta = 0$, and vanishes for $\eta = 1$.

Definition 2.2 The iterated solution to the given model of fractional order $\eta \in [0, 1]$ is given by.

$$\text{ABC } D_{0+}^{\eta}\,\text{f(t)} = f_0 + \frac{1-\eta}{M(\eta)}\text{f(t)} + \frac{\eta}{M(\eta)\Gamma\eta}\int_0^t (t-y)^{\eta-1}\text{f(y)}\,\text{dy} \tag{4}$$

where ABC D_{0+}^{η} f(t) is the η-*order* fractional derivative of ABC type, f_0-initial value of the function f(t).

Schauder's Fixed Point Theorem [49]

For a non-empty closed and convex subset N of a Banach space H. Let us assume a continuous map N onto a relatively compact f (N) $\subset$ H, then there exists a unique fixed point in N, (i.e.)

$$\text{f (x)} = \text{x for x} \in \text{N}.$$

Krasnoselski Fixed Point Theorem [49]

Let N $\neq \phi$, closed and convex subset of a Banach space (H, $\|.\|$), T_1 and T_2 maps N into S such that,

(i) T_1x + T_2 y $\in$ N for all values x, y *in* N.
(ii) T_1 is continuous, T_1 N $\subset$ N, which is compact in H.
(iii) A contraction map T_2, satisfying T_1 x + T_2 x = x.

Definition

A solution x = φ(t) of (1) is,

(i) attractive if the zero solution $\varphi(t) = 0$ such that $\|x_0\| \leq \varepsilon, \Rightarrow \lim_{t\to\infty} x_0 = 0$.
(ii) Attractive and stable $\Rightarrow$ asymptotic stability.

Formulation of Mathematical Model $\mathcal{SVIP}$

The mathematical disease model in this study is framed using references therein [43–48] with various control measures. It has been noted that apart from susceptible infections, inefficient vaccinated infections are also possible and taken into count. Many are found to be well protected due to self-preventive actions which are non-medicinal. Each new infants are suscepted significantly to get contagious also considered. The sum of persons into account

is N$(t) = \mathcal{S} + \mathcal{V} + \mathcal{I} + P$. The entire strength is split up into four distinct sub-individuals as follows:

(i) Susceptible population $\mathcal{S}(t)$: The class of unvaccinated susceptible persons to get infected at any time.
(ii) Vaccinated population $\mathcal{V}(t)$: The class of vaccinated people, susceptible to get infected in case of vaccine inefficacy.
(iii) Infected population $\mathcal{I}(t)$: The class of infected persons both from unvaccinated and vaccinated susceptibles.
(iv) Protected population $P(t)$: The class of self protected susceptibles and those recovered from infection.

Assumptions of the parameters involved in the model:

(i) Total population of the contaminated region under study be assumed as $(N(t))$.
(ii) The persons entering the susceptible population $\mathcal{S}(t)$ were assumed as 'a'
(iii) Let 'v' be the proportion of vaccinated individuals with the total probability $0 < \mathrm{v} \leq 1$. The unvaccinated persons 'va' from $\mathcal{S}(t)$ gets vaccinated and move on to $\mathcal{V}(t)$.
(iv) Infection rate of susceptibles $\frac{\beta}{N}$ moves into $\mathcal{I}(t)$.
(v) Infection rate of vaccinated individuals $\frac{\alpha}{N}$ due to vaccine inefficacy added to infected group $\mathcal{I}(t)$.
(vi) Natural death occurring among all individuals denoted by μ.
(vii) Due to severe complications of the disease, mortality of infected persons denoted by ϕ removed from $\mathcal{I}(t)$.
(viii) Natural immunity gained due to recovery from infection is assumed as γ, moves to $P(t)$.
(ix) Even protected individuals $P(t)$ gets infected at the rate of δ, enters in $\mathcal{I}(t)$.
(x) Rate of self -preventive practices defending from infection is denoted as Ψ, added to $P(t)$.

The novel vaccination model with personal precautions for Covid-19 with the notations discussed above is formulated in the commensurate system (5) in terms of equal ABC fractional order 'η'.

$$\left.\begin{aligned} ABC\ D^{\eta}_{0+}\mathcal{S}(t) &= (1-\mathrm{v})\mathrm{a} - \tfrac{\beta\mathcal{S}\mathcal{I}}{N} - \mu\mathcal{S} - \Psi\mathcal{S} \\ ABC\ D^{\eta}_{0+}\mathcal{V}(\mathrm{t}) &= \mathrm{va} - \tfrac{\alpha\mathcal{V}\mathcal{I}}{N} - \mu\mathcal{V} \\ ABC\ D^{\eta}_{0+}\mathcal{I}(t) &= \tfrac{\beta\mathcal{S}\mathcal{I}}{N} + \tfrac{\alpha\mathcal{V}\mathcal{I}}{N} - \mu\mathcal{I} - \gamma\mathcal{I} - \phi\mathcal{I} + \delta P \\ ABC\ D^{\eta}_{0+}P(\mathrm{t}) &= \gamma\mathcal{I} + \Psi\mathcal{S} - \mu P - \delta P \end{aligned}\right\} \tag{5}$$

where $0 < \eta < 1$, ABC D^{η}_{0+} is the ABC derivative of order η, with the initial conditions $\mathcal{S}(0)$, $\mathcal{V}(0)$, $\mathcal{I}(0)$, $P(0)$ are all non-negative (Table 1).

Basic Properties of the Model

Equilibrium Point Analysis [44, 46, 50]

By solving the commensurate model [48] of same order η, we obtain two state of equilibrium as follows,

Infection free equilibrium (IFE):

Table 1 Numerical data for the parameters

Parameters	Description	Value
N	Total population	1401.23 in millions
$\boldsymbol{S}_0$	Initial susceptible population	0.0031941
$\boldsymbol{V}_0$	Initial susceptible population	0.000392
$\boldsymbol{I}_0$	Initial susceptible population	0.0003543
$\boldsymbol{P}_0$	Initial protected population	0.00033
a	Total recruitment rate	0.06987
v	Rate of Initial vaccination	0.000492
β	Transmission rate of susceptibles	1100.01, 1000.00, 800.13
α	Infection rate of vaccinated susceptibles	310, 200.123, 0
γ	Recovery rate from disease	0.003
δ	Relapse rate of protected individuals	0.00033
μ	Natural death rate	0.00002
ϕ	Disease induced death rate	0.00003
Ψ	Self-prevention rate of protected population	0.0261, 0.051, 0.078, 1

Assuming the infections in (5) to be zero we derive the infection free point,

$$'\mathrm{E}_0(\mathcal{S}_0, \mathcal{V}_0, \mathcal{I}_0, P_0) = \left(\frac{(1-v)a}{\mu+\Psi}, \frac{va}{\mu}, 0, \frac{\Psi(1-v)a}{(\mu+\Psi)(\mu+\delta)}\right), \quad \text{if } \mathcal{I}=0 \tag{6}$$

Infection persistent equilibrium (IPE):

In view of, continuous prevalence of infective cases, the values of IPE given by $\mathcal{S}_p, \mathcal{V}_p, \mathcal{I}_p, P_p$ derived from (5) follows,

$$'\mathrm{E}_p\left(\mathcal{S}_p, \mathcal{V}_p, \mathcal{I}_p, P_p\right) = \left(\frac{(1-v)a}{\beta\mathcal{I}+(\mu+\Psi)N_{0,}}N_{0,}, \frac{va}{\alpha\mathcal{I}+\mu N_{0,}}N_{0,}, \mathcal{I}_p, \frac{\gamma\mathcal{I}+\Psi\mathcal{S}}{(\mu+\delta)}\right) \text{ if } \mathcal{I}\neq 0. \tag{7}$$

Stability and Sensitivity Around the Threshold Metric

Theorem 4.1.2 *The threshold value* $R_0 = \beta\mathcal{S}+\alpha\mathcal{V}-N_0(\mu+\gamma+\phi)$ *is the pandemic metric of secondary infections transmitted from an infected person, then the framed model* (5)

(i) *remains stable if* $R_0 = \frac{\beta(1-v)a}{(\mu+\gamma+\phi)(\mu+\Psi)N_0} + \frac{\alpha(va)}{(\mu+\gamma+\phi)\mu N_{0,}} < 1$, *observing the controllability of the disease.*

(ii) *will be persistently unstable if* $R_0 > 1$.

Proof The stability of infection free state $'\mathrm{E}_0$ can be examined by deriving the next generation matrix FV^{-1}, for system (5). By arraying the new positive infective cases of (5) in the matrix F and migration of infected to other compartments as V, we get,

$$F = \begin{pmatrix} \frac{\beta\mathcal{S}+\alpha\mathcal{V}}{N} & 0 \\ 0 & 0 \end{pmatrix}, \quad V = \begin{pmatrix} 0 \\ \mu+\gamma+\phi \end{pmatrix}$$

The largest spectral radius, $\rho(FV^{-1})$ is the epidemic threshold parameter,

$$R_0 = \beta\mathcal{S}+\alpha\mathcal{V}-N_0(\mu+\gamma+\phi) \tag{8}$$

(i) The (IFE) $'E_0$ exhibits that, a rapid control of the disease will happen only if,

$$\frac{\beta(1-v)a}{\beta\mathcal{I}+(\mu+\Psi)N_{0,}}+\frac{\alpha(va)}{\alpha\mathcal{I}+\mu N_{0,}}-N_0(\mu+\gamma+\phi)<1. \tag{9}$$

(ii) Analysing the infection prevalent state, the stability around the (IPE) $'E_p$ point,
From (7) we have $\left(\frac{\beta(1-v)a}{\beta\mathcal{I}+(\mu+\Psi)N_{0,}}+\frac{\alpha(va)}{\alpha\mathcal{I}+\mu N_{0,}}-N_0(\mu+\gamma+\phi)\right)\mathcal{I}+\delta P N_0=0$

$$\mathcal{I}\neq 0,\ \text{Then}\ \left(\frac{\beta(1-v)a}{\beta\mathcal{I}+(\mu+\Psi)N_{0,}}+\frac{\alpha(va)}{\alpha\mathcal{I}+\mu N_{0,}}-N_0(\mu+\gamma+\phi)\right)\mathcal{I}=-\delta P N_0 \tag{10}$$

$\mathcal{I}_p=\frac{\beta(1-v)a}{\beta\mathcal{I}+(\mu+\Psi)N_{0,}}+\frac{\alpha(va)}{\alpha\mathcal{I}+\mu N_{0,}}\leq N_0(\mu+\gamma+\phi-\delta P)$, then the disease spread in the region will prevail persistently.

Sensitivity Analysis

Sensitivity analysis are very useful and highly supported by eco-epidemiologists to identify the alleviating factors of contagious spread. Sensitivity ratios were calculated partially differentiating with respect to every parameters of the threshold value R_0. This suggests a comparative study on impacts and effects of the parameters defining the disease dynamics. These indices influence all the primary note about the transmission, reduction and control of the viral parasites.

Definition 4.2.1 The threshold value R_0 defines the sensitivity ratio by partial derivatives of its every parameter, $\mathfrak{S}_{\varpi}=\frac{\partial R_0}{\partial\varpi}\frac{\varpi}{R_0}$, where ϖ- assumes all the parameters defining R_0.

The reproduction ratio plays a significant role in predicting the control of an ailment. From the fied data of Covid-19 in India, R_0 were very high ranging between 2 and 3 in the emerging months of 2020. It started to decline reaching a local maximum after 7 months reporting stability and control with $R_0=0.99$ in Mid October 2020. There was a sudden hike recorded in early days of 2021, due to contagiousness of the microparasites. Moreover, the positive consequences of rapid vaccination and self-protectiveness helps to reduce the infection spread later at the end of 2021. Still there were instable peak caused due to seasonal changes in Dec 2021 [51].

By differentiating directly R_0, The sensitivity relation between all parameters from (8), (9) are calculated and interpreted with numerical values as follows in Table 2.

$$\frac{\partial R_0}{\partial\beta}\frac{\beta}{R_0}=\frac{\beta\mathcal{S}}{\beta\mathcal{S}+\alpha\mathcal{V}};\quad \frac{\partial R_0}{\partial\alpha}\frac{\alpha}{R_0}=\frac{\alpha\mathcal{V}}{\beta\mathcal{S}+\alpha\mathcal{V}};$$
$$\frac{\partial R_0}{\partial\Psi}\frac{\Psi}{R_0}=-\frac{[\alpha\mathcal{V}+\mu\beta(1-v)]a}{[\mu\beta(1-v)a+\alpha(va)(\mu+\Psi)]};$$
$$\frac{\partial R_0}{\partial\phi}\frac{\phi}{R_0}=-\frac{\phi}{N_0(\mu+\gamma+\phi)};\quad \frac{\partial R_0}{\partial a}\frac{a}{R_0}=\frac{1}{N_0(\mu+\gamma+\phi)}\left(\frac{\beta(1-v)}{(\mu+\Psi)}+\frac{\alpha v}{\mu}\right)$$
$$\frac{\partial R_0}{\partial v}\frac{v}{R_0}=\frac{v[\alpha a(\mu+\Psi)-\mu a\beta]}{[\mu\beta(1-v)a+\alpha(va)(\mu+\Psi)]};\quad \frac{\partial R_0}{\partial\mu}\frac{\mu}{R_0}=-\frac{\mu}{(\mu+\gamma+\phi)}$$
$$\frac{\partial R_0}{\partial\gamma}\frac{\gamma}{R_0}=-\frac{\gamma}{N_0(\mu+\gamma+\phi)}$$

The relation between the disease spread and the parameters explaining the behaviour of viral pathogens were interpreted which helps to design and implement effective control steps.

Table 2 Sensitivity indices for numerical input from Table 1

Parameters	Sensitivity index	Value
$\boldsymbol{a}$	$\mathfrak{S}_a$	6.9114
v	$\mathfrak{S}_v$	0.45963
β	$\mathfrak{S}_{\boldsymbol{\beta}}$	0.94291
α	$\mathfrak{S}_{\boldsymbol{\alpha}}$	0.0571
γ	$\mathfrak{S}_{\boldsymbol{\gamma}}$	− 0.98361
μ	$\mathfrak{S}_{\boldsymbol{\mu}}$	− 0.00656
ϕ	$\mathfrak{S}_{\boldsymbol{\phi}}$	− 0.00984
Ψ	$\mathfrak{S}_{\boldsymbol{\Psi}}$	− 0.525687

From the above table, the parameters a,v, β, α, Ψ shows a direct positive dominance over the pandemic threshold value R_0 which implicates the magnification or lessening of these parameters reacts more sensitive to reproduction number R_0. For instance, increasing the values by 10(say), we have $a = 69.114$, $\mathrm{v} = 4.5963$, $\beta = 9.4291$, $\alpha = 0.571$, will sensitively hyperbolize R_0. Nevertheless, the negative sensitivity ratio with respect to recovery rate $\boldsymbol{\gamma}$ $= 9.8361$, natural death rate $\mu = 0.0656$ and disease death rate $\phi = 0.0984$, self- protective rate, $\Psi = 5.2568$ contradicts the increment of 10 resulting in decrement of the metric R_0. Thus by increasing the rate of vaccination, self-prevention results in better controllability of the pandemic spread.

Stability analysis

The stable condition of the equilibrium points is investigated in this section. To its key note, the Jacobian matrix of (5) is arrayed as,

$$J = \begin{pmatrix} -\left(\frac{\beta\mathcal{I}}{N} + \mu + \Psi\right) & 0 & -\frac{\beta\mathcal{S}}{N} & 0 \\ 0 & -\frac{\alpha\mathcal{I}}{N} - \mu & -\frac{\alpha\mathcal{V}}{N} & 0 \\ \frac{\beta\mathcal{I}}{N} & \frac{\alpha\mathcal{I}}{N} & \frac{\beta\mathcal{S}+\alpha\mathcal{V}}{N} - \mu - \gamma - \phi & \delta \\ \Psi & 0 & \gamma & -\delta - \mu \end{pmatrix}$$

Local stability of infection-free equilibrium (IFE)

Theorem 4.3.1 *The infection free equilibrium (IFE) point* $\left(\frac{(1-v)a}{\mu+\Psi}, \frac{va}{\mu}, 0, \frac{\Psi(1-v)a}{(\mu+\Psi)(\mu+\delta)}\right)$ *exhibits local asymptotic stability if* $R_0 < 1$ *and unstable if* $R_0 > 1$.

Proof The model (5) is linearized by deriving the partial derivatives to form the Jacobian form.

The Jacobian matrix about (IFE) is arrayed as,

$$\mathrm{J}(\mathrm{'E_0}) = \begin{pmatrix} -(\mu + \Psi) & 0 & -\frac{\beta}{N}\frac{(1-v)a}{\mu+\Psi} & 0 \\ 0 & -\mu & -\frac{\alpha\mathcal{V}}{N} & 0 \\ 0 & 0 & \frac{\beta\frac{(1-v)a}{\mu+\Psi}+\alpha\frac{va}{\mu}}{N} - \mu - \gamma - \phi & \delta \\ \Psi & 0 & \gamma & -\delta - \mu \end{pmatrix}$$

The eigen roots of the above matrix are obtained from its characteristic equation.

$$|\mathrm{J}('\mathrm{E}_0)-\lambda I|=\begin{vmatrix} -(\mu+\Psi)-\lambda & 0 & -\frac{\beta}{N}\frac{(1-v)a}{\mu+\Psi} & 0 \\ 0 & -\mu-\lambda & -\frac{\alpha}{N}\frac{va}{\mu} & 0 \\ 0 & 0 & \left(\frac{\beta\frac{(1-v)a}{\mu+\Psi}+\alpha\frac{va}{\mu}}{N}-(\mu+\gamma+\phi)\right)-\lambda & \delta \\ \Psi & 0 & \gamma & (-\delta-\mu)-\lambda \end{vmatrix}=0$$

yields $\lambda_1=(\mu+\Psi)$, $\lambda_2=\mu$ and roots of $\lambda^{\,2}+\mathrm{k}_1\lambda+\mathrm{k}_2=0$, where

$$\mathrm{k}_1=-\left(\frac{\beta\frac{(1-v)a}{\mu+\Psi}+\alpha\frac{va}{\mu}}{N}-(2\mu+\gamma+\phi+\delta)\right),$$

$$\mathrm{k}_2=-\left[(\delta+\mu)\left(\frac{\beta\frac{(1-v)a}{\mu+\Psi}+\alpha\frac{va}{\mu}}{N}-(\mu+\gamma+\phi)\right)+\delta\gamma\right]$$

For the controllability of infection if $R_0<1$ with all the non-negative parameters, we have the roots with negative principal parts.

$$\mathrm{k}_1=\frac{\beta\frac{(1-v)a}{\mu+\Psi}+\alpha\frac{va}{\mu}}{N}-(2\mu+\gamma+\phi+\delta)<0,\ \frac{\beta\frac{(1-v)a}{\mu+\Psi}+\alpha\frac{va}{\mu}}{N}<(2\mu+\gamma+\phi+\delta)\Rightarrow \mathrm{k}_1>0.$$

$$\mathrm{k}_2=(\delta+\mu)\left(\frac{\beta\frac{(1-v)a}{\mu+\Psi}+\alpha\frac{va}{\mu}}{N}-(\mu+\gamma+\phi)\right)+\delta\gamma<0$$

$$\left(\frac{\beta\frac{(1-v)a}{\mu+\Psi}+\alpha\frac{va}{\mu}}{N}\right)+\frac{\delta\gamma}{(\delta+\mu)}<(\mu+\gamma+\phi)\Rightarrow \mathrm{k}_2>0.$$

By Routh–Hurwitz criterion, the system (5) is stable around the $'\mathrm{E}_0$, if $R_0<1$ and unstable if any of the real eigen-root is positive.

The unstability $R_0>1$ of the IFE point occurs if $\mathrm{k}_2<0\Rightarrow{}'\mathrm{E}_0$ is unstable.

Local stability of infection-persistent equilibrium (IPE)

The IPE is the steady-state point at which the infection spread persists still among the people. For non-zero positive values of $'\mathrm{E}_p(\mathcal{S}_p,\mathcal{V}_p,\mathcal{I}_p,P_p)$, let us obtain the Jacobian and its characteristic values.

$$J('\mathrm{E}_p)=\begin{pmatrix} -\left(\frac{\beta\mathcal{I}_p}{N}+\mu+\Psi\right) & 0 & -\frac{\beta\mathcal{S}_p}{N} & 0 \\ 0 & -\frac{\alpha\mathcal{I}_p}{N}-\mu & -\frac{\alpha\mathcal{V}_p}{N} & 0 \\ \frac{\beta\mathcal{I}_p}{N} & \frac{\alpha\mathcal{I}_p}{N} & \frac{\beta\mathcal{S}_p+\alpha\mathcal{V}_p}{N}-\mu-\gamma-\phi & \delta \\ \Psi & 0 & \gamma & -\delta-\mu \end{pmatrix}$$

The eigenvalues of the above Jacobian are obtained from its characteristic equation.

$$
\begin{aligned}
&|\mathrm{J}('\mathrm{E}_p) - \lambda I| \\
&= \begin{vmatrix} -\left(\frac{\beta \mathcal{I}_p}{N} + \mu + \Psi\right) - \lambda & 0 & -\frac{\beta \mathcal{S}_p}{N} & 0 \\ 0 & -\left(\frac{\alpha \mathcal{I}_p}{N} + \mu\right) - \lambda & -\frac{\alpha \mathcal{V}_p}{N} & 0 \\ \frac{\beta \mathcal{I}_p}{N} & \frac{\alpha \mathcal{I}_p}{N} & \left(\frac{\beta \mathcal{S}_p + \alpha \mathcal{V}_p}{N} - (\mu + \gamma + \phi)\right) - \lambda & \delta \\ \Psi & 0 & \gamma & (-\delta - \mu) - \lambda \end{vmatrix} \\
&= 0
\end{aligned}
$$

The roots of $\lambda^3 - l_1\lambda^2 + l_2\lambda - l_3 = 0$ and $\lambda = -(\delta + \mu)$ are the eigen values of $\mathrm{J}('\mathrm{E}_p)$ with

$$
\begin{aligned}
l_1 &= -\left(\frac{\beta \mathcal{S}_p - \beta \mathcal{I}_p + \alpha \mathcal{V}_p}{N} - (3\mu + \gamma + \Psi + \phi)\right) \\
l_2 &= \frac{1}{N}\begin{bmatrix} \mathcal{I}_p\left(\alpha(\gamma + \phi - \Psi) + \beta(\gamma + \phi) - \frac{\alpha\beta}{N}\left(\mathcal{S}_p + \mathcal{V}_p - \mathcal{I}_p\right)\right) \\ -\Psi\left(\alpha \mathcal{S}_p + \beta \mathcal{V}_p\right) - 2\mu\left(\alpha \mathcal{V}_p + \beta \mathcal{S}_p - \beta \mathcal{I}_p\right) \end{bmatrix} \\
&\quad + \mu\left[3(\mu + \Psi) + 2\gamma + \phi)\right] + \Psi(\gamma + \phi) \\
l_3 &= -\frac{1}{N}\left\{ \begin{bmatrix} \frac{\alpha\beta \mathcal{I}_p}{N}\left(\mu\left(\mathcal{S}_p + \mathcal{V}_p\right)\right) + \Psi \mathcal{S}_p - (\mu + \gamma + \phi)\mathcal{I}_p \end{bmatrix} + \Psi\left[\mu\left(\alpha \mathcal{V}_p + \beta \mathcal{S}_p\right) - \alpha \mathcal{I}_p(\gamma + \phi)\right] \right\} \\
&\quad \begin{bmatrix} -\mu \mathcal{I}_p\left[(\alpha + \beta)(\gamma + \phi) + \Psi\alpha\right] - \mu^2\left[(\alpha + \beta)\mathcal{I}_p - \left(\alpha \mathcal{V}_p + \beta \mathcal{S}_p\right)\right] \end{bmatrix} \\
&\quad - \mu^2\left[(\mu + \gamma + \phi + \Psi)\right] - \Psi\mu(\gamma + \phi)
\end{aligned}
$$

The coefficients of the characteristic equation reveals that system (5) is locally asymptotic stable around the infection persistent point $'\mathrm{E}_p$, if $l_1\, l_2 < l_3$ and unstable if any of the real eigen-root is positive with $l_1\, l_2 > l_3$.

Positivity, feasible adherence and persistence

This section ensures the positive and feasible well-posedness of the bio-mathematical model (5) for every initial value set $(\mathcal{S}(0), \mathcal{V}(0), \mathcal{I}(0), P(0))$ defined on [0, 1).

Lemma 4.4.1 *Positivity and Feasible adherence*
The eigen value solution $(\mathcal{S}, \mathcal{V}, \mathcal{I}, P)$ *of* (5) *hold the following,*

(i) *For the non-negative initial values of the subgroups defined in* (1) *satisfying* $\mathcal{S}(0) > 0, \mathcal{V}(0) > 0, \mathcal{I}(0) > 0, P(0) > 0$, *we have an unique perturbated solution* $\mathcal{S}(t) > 0, \mathcal{V}(t) > 0, \mathcal{I}(t) > 0, P(t) > 0$ *defined in* [0, 1).
(ii) *The eigen value solution* $(\mathcal{S}, \mathcal{V}, \mathcal{I}, P)$ *of* (5) *is adherely bounded in the feasible region.*

$\left\{(\mathcal{S}, \mathcal{V}, \mathcal{I}, P) \epsilon R^4\right\}, o < N(t) \leq \frac{a}{\mu}$, *where* $N(t) = \mathcal{S} + \mathcal{V} + \mathcal{I} + P$.

Proof The proof of (i) assumes the potential state of all variables,

At $\mathcal{S} = 0$, ABC $D^{\eta}_{0+}\mathcal{S}(t) = (1 - \mathrm{v})\mathrm{a} \geq 0$
At $\mathcal{V} = 0$, ABC $D^{\eta}_{0+}\mathcal{V}(t) = \mathrm{va} \geq 0$
At $\mathcal{I} = 0$, ABC $D^{\eta}_{0+}\mathcal{I}(t) = \delta P \geq 0$
At $P = 0$, ABC $D^{\eta}_{0+}P(t) = \gamma\mathcal{I} + \Psi\mathcal{S} \geq 0$
Hence the variables defined by $\left\{(\mathcal{S}, \mathcal{V}, \mathcal{I}, P) \epsilon R^4\right\}$ are all non-negative.

To prove the part (ii), Adding all the sub-populations of (1), we have

$$\begin{aligned}\sum \text{ABC } D^{\eta}_{0+}(\mathcal{S}, \mathcal{V}, \mathcal{I}, P) &= \text{ABC } D^{\eta}_{0+}N(t)\\ &\leq a - \mu N(t) - \phi\mathcal{I}(t)\\ \text{ABC } D^{\eta}_{0+}N(t) &\leq a - \mu N(t)\end{aligned}$$

Integrating upon both sides, we get

$$\begin{aligned}N(t) &= -\frac{a}{\mu}e^{-\mu t} + \frac{a}{\mu} + N(0)e^{-\mu t}\\ &= \frac{a}{\mu}\left(1 - e^{-\mu t}\right) + N(0)e^{-\mu t},\end{aligned}$$

which yields some positive constant.

Hence for infinitely large time t, The feasible adherent least upper bound of $N(t)) \leq \frac{a}{\mu}$.

Persistence of the ailment

The persistence of the ailment for a long period is exhibited in this lemma.

Lemma 4.4.2 *Let $\langle t_n\rangle$ be a sequence of time prevalence of the epidemic system, as* $\mathrm{n} \to \infty$, $\mathcal{S}(t_n) \to \mathrm{f}$, $\mathcal{V}(t_n) \to g$, $\mathcal{I}(t_n) \to 0$ *and* $P(t_n) \to \mathrm{h}$, *then for every solution* $(\mathcal{S}, \mathcal{V}, \mathcal{I}, P)$ *of the model* (5) *we have,*

$$f = \frac{(1-v)a}{\mu+\Psi}, g = \frac{va}{\mu}, h = \frac{\Psi(1-v)a}{(\mu+\Psi)(\mu+\delta)}.$$

Proof Let us assume a sequence $\langle t_n\rangle$ of time, the disease spread continues to persists in a region.

From Lemma 4.4.1, it is clear that, $\frac{(1-v)a}{\mu+\Psi} \geq f \geq 0$, $\frac{va}{\mu} \geq g \geq 0$ and $\frac{\Psi(1-v)a}{(\mu+\Psi)(\mu+\delta)} \geq h \geq 0$ for infinitely large t, subject to the vanishing infections $\mathcal{I}(t_n) \to 0$.

Let the solution $(\mathcal{S}, \mathcal{V}, \mathcal{I}, P)$ of (5) belongs to the limit point invariant set,

$$\varpi = \left\{(\mathcal{S}, \mathcal{V}, \mathcal{I}, P) \epsilon R^4, o < N(t) \leq \frac{a}{\mu}\right\}, \text{ where } N(t) = \mathcal{S} + \mathcal{V} + \mathcal{I} + P.$$

The limit value $(f, g, 0, h) \in \left(\mathcal{S}_0, \mathcal{V}_0, \mathcal{I}_0, P_0\right)$, for every $(\mathcal{S}, \mathcal{V}, \mathcal{I}, P) \in \omega$, as $n \to \infty$.

It follows that, for every $t \in [0, \mathrm{T}] \subset R$, $\mathcal{S}(t) = \mathcal{S}_0 + \left(f - \frac{1}{\frac{\mu+\Psi}{(1-v)a}}\right)e^{-\left(\frac{(1-v)a}{\mu+\Psi}\right)t}$.

$$\mathcal{V}(t) = \mathcal{V}_0, + \left(g - \frac{1}{\frac{\mu}{va}}\right)e^{-\left(\frac{va}{\mu}\right)t}, P(t) = P_0 + \left(h - \frac{1}{\frac{(\mu+\Psi)(\mu+\delta)}{\Psi(1-v)a}}\right)e^{-\left(\frac{\Psi(1-v)a}{(\mu+\Psi)(\mu+\delta)}\right)t}, \mathcal{I}(t) = 0.$$

On contradicting the fact of non-negativity of all values, $\mathcal{S}(t)$, $\mathcal{V}(t)$ and $P(t)$ turns negative when $t_n \to -\infty$.

Unique solution existence

Existence of unique solution is guaranteed by functional analysis of non-linear functions defined on a Banach space. Theorem of fixed point indicates the considered model (5) possess atleast single solution in [0, T].

Let us consider, L$(t, \mathcal{S})$, M$(t, \mathcal{V})$, N$(t, \mathcal{I})$, O(t, P) are continuous kernel functions with respect to $\mathcal{S}(t)$, $\mathcal{V}(t)$, $\mathcal{I}(t)$ and $P(t)$ respectively.

$$\left.\begin{aligned} ABC\ D^{\eta}_{0+}S(t) &= (1-\mathrm{v})a - \tfrac{\beta\mathcal{S}\mathcal{I}}{N} - \mu S - \Psi S = L(t,\mathcal{S}) \\ ABC\ D^{\eta}_{0+}V(t) &= va - \tfrac{\alpha\mathcal{V}\mathcal{I}}{N} - \mu V = M(t,\mathcal{V}) \\ ABC\ D^{\eta}_{0+}I(t) &= \tfrac{\beta\mathcal{S}\mathcal{I}}{N} + \tfrac{\alpha\mathcal{V}\mathcal{I}}{N} - \mu I - \gamma I - \phi I + \delta P = N(t,\mathcal{I}) \\ ABC\ D^{\eta}_{0+}P(t) &= \gamma I + \Psi S - \mu P - \delta P = O(t,P) \end{aligned}\right\} \tag{11}$$

Reformulation of (11) in the form of AB integral as expressed in (4) are given by,

$$\left.\begin{aligned} \mathcal{S}(t) &= \mathcal{S}_0 + \tfrac{1-\eta}{M(\eta)}\,\mathrm{L}(t,\mathcal{S}(t)) + \tfrac{\eta}{M(\eta)\Gamma\eta}\int_0^t (t-y)^{\eta-1}\mathrm{L}(\mathrm{y},\mathcal{S}(\mathrm{y}))\mathrm{dy} = L_1 + L_2 \\ \mathcal{V}(t) &= \mathcal{V}_0 + \tfrac{1-\eta}{M(\eta)}M(t,\mathcal{V}(t)) + \tfrac{\eta}{M(\eta)\Gamma\eta}\int_0^t (t-y)^{\eta-1}M(y,\mathcal{V}(y))dy = M_1 + M_2 \\ \mathcal{I}(t) &= \mathcal{I}_0 + \tfrac{1-\eta}{M(\eta)}\,\mathrm{N}(t,\mathcal{I}(t)) + \tfrac{\eta}{M(\eta)\Gamma\eta}\int_0^t (t-y)^{\eta-1}\mathrm{N}(\mathrm{y},\mathcal{I}(\mathrm{y}))\mathrm{dy} = N_1 + N_2 \\ P(t) &= P_0 + \tfrac{1-\eta}{M(\eta)}\,\mathrm{O}(t,P(t)) + \tfrac{\eta}{M(\eta)\Gamma\eta}\int_0^t (t-y)^{\eta-1}\mathrm{O}(\mathrm{y},P(\mathrm{y}))\mathrm{dy} = O_1 + O_2 \end{aligned}\right\} \tag{12}$$

For the real world applications of nonlinear functional system, the existence of the model is proved with the help of fixed point theorems. In the point of Krasnoselski's theorem on fixed point, let us group the governing equations (12) and prove them as contraction maps $\mathbf{A}\big(L_1, M_1, N_1, O_1\big)$ and $\mathbf{B}(L_2, M_2, N_2, O_2)$ of continuous compact integrals, where

$$L_1 = \mathcal{S}_0 + \frac{1-\eta}{M(\eta)}L(t,\mathcal{S}(t)),\ L_2 = \frac{\eta}{M(\eta)\Gamma\eta}\int_0^t (t-y)^{\eta-1}\mathrm{L}(\mathrm{y},\mathcal{S}(\mathrm{y}))\mathrm{dy}$$

$$M_1 = \mathcal{V}_0 + \frac{1-\eta}{M(\eta)}M(t,\mathcal{V}(t)),\ M_2 = \frac{\eta}{M(\eta)\Gamma\eta}\int_0^t (t-y)^{\eta-1}\mathrm{M}(\mathrm{y},\mathcal{V}(\mathrm{y}))\mathrm{dy}$$

$$N_1 = \mathcal{I}_0 + \frac{1-\eta}{M(\eta)}\mathrm{N}(t,\mathcal{I}(t)),\ N_2 = \frac{\eta}{M(\eta)\Gamma\eta}\int_0^t (t-y)^{\eta-1}\mathrm{N}(\mathrm{y},\mathcal{I}(\mathrm{y}))\mathrm{dy}$$

$$O_1 = P_0 + \frac{1-\eta}{M(\eta)}\,\mathrm{O}(t,P(t)),\ O_2 = \frac{\eta}{M(\eta)\Gamma\eta}\int_0^t (t-y)^{\eta-1}\mathrm{O}(\mathrm{y},P(\mathrm{y}))\mathrm{dy} \tag{13}$$

Theorem 4.5.1 *The non-linear maps* $\mathbf{A}\big(L_1, M_1, N_1, O_1\big)$:[0, T] x R x R x R $\to$ R^4 *defined in* (8) *satisfy the Lipschitzian contractive condition for constants* $K_L, K_M, K_N, K_O > 0$.

Proof Let the operators $\mathbb{A}\big(L_1, M_1, N_1, O_1\big)$:[0, T] x R x R x R $\to$ R^4, defined on a complete normed linear space with norm,

$$\|(\mathcal{S},\mathcal{V},\mathcal{I},P)\| = \max_{t\in[0,T]}\{\|\mathcal{S}(t)+\mathcal{V}(t)+\mathcal{I}(t)+P(t)\|\}\text{where } \mathcal{S},\mathcal{V},\mathcal{I},P \in [0,\mathrm{T}].$$

First let us prove that $\mathbf{A}\left(L_1, M_1, N_{1,} O_1\right)$ is a contraction map.

For $\mathcal{S}(t)$ and $\hat{\mathcal{S}}(t)$, we have.

$$\left\|\mathrm{L}(\mathcal{S}, \mathcal{V}, \mathcal{I}, P)(t) - \mathrm{L}\left(\widehat{\mathcal{S}}, \widehat{\mathcal{V}}, \hat{\mathcal{I}}, \widehat{P}\right)(t)\right\|$$

$$= \left\|(1-\mathrm{v})\mathrm{a} - \frac{\beta\mathcal{S}\mathcal{I}}{N} - \mu\mathcal{S} - \Psi\mathcal{S} - (1-\mathrm{v})\mathrm{a} + \frac{\beta\widehat{\mathcal{S}}\mathcal{I}}{N} + \mu\hat{\mathcal{S}} + \Psi\mathcal{S}\right\|$$

$$= \left\|\frac{\beta\mathcal{I}}{N}\left(\mathcal{S} - \hat{\mathcal{S}}\right) - \mu\left(\mathcal{S} - \hat{\mathcal{S}}\right) - \Psi\left(\mathcal{S} - \hat{\mathcal{S}}\right)\right\|$$

$$\left\|\mathrm{L}(\mathcal{S}, \mathcal{V}, \mathcal{I}, P)(t) - \mathrm{L}\left(\widehat{\mathcal{S}}, \widehat{\mathcal{V}}, \hat{\mathcal{I}}, \widehat{P}\right)(t)\right\|$$

$$\leq \left\|\left(\frac{\beta\mathcal{I}}{N} + \mu + \Psi\right)\left\|\mathcal{S} - \hat{\mathcal{S}}\right\|\right\|$$

$$\leq \left\|\left(\frac{\beta\mathcal{I}}{N} + \mu + \Psi\right)\right\|\left\|\mathcal{S} - \hat{\mathcal{S}}\right\|$$

$$\left\|\mathrm{L}(\mathcal{S}, \mathcal{V}, \mathcal{I}, P)(t) - \mathrm{L}\left(\widehat{\mathcal{S}}, \widehat{\mathcal{V}}, \hat{\mathcal{I}}, \widehat{P}\right)(t)\right\| \leq K_L\left\|\mathcal{S} - \hat{\mathcal{S}}\right\|, \text{ where } K_L = \left(\frac{\beta\mathcal{I}}{N} + \mu + \Psi\right)$$

Similarly for other mappings, M,N,O we derive,

$$\left\|\mathrm{M}(\mathcal{S}, \mathcal{V}, \mathcal{I}, P)(t) - \mathrm{M}\left(\widehat{\mathcal{S}}, \widehat{\mathcal{V}}, \hat{\mathcal{I}}, \widehat{P}\right)(t)\right\| \leq K_M\left\|\mathcal{V} - \hat{\mathcal{V}}\right\|, \text{ where } K_M\Big\| = \left(\frac{\alpha}{N}\|\mathcal{I}\| + \mu\right)\Big\|$$

$$\left\|\mathrm{N}(\mathcal{S}, \mathcal{V}, \mathcal{I}, P)(t) - N\left(\widehat{\mathcal{S}}, \widehat{\mathcal{V}}, \hat{\mathcal{I}}, \widehat{P}\right)(t)\right\| \leq K_N\left\|\mathcal{I} - \hat{\mathcal{I}}\right\|, \text{ where } K_N = \left\|\left(\frac{\beta\mathcal{S} + \alpha\mathcal{V}}{N} + \mu + \gamma + \phi\right)\right\|$$

$$\left\|\mathrm{O}(\mathcal{S}, \mathcal{V}, \mathcal{I}, P)(t) - \mathrm{O}\left(\widehat{\mathcal{S}}, \widehat{\mathcal{V}}, \hat{\mathcal{I}}, \widehat{P}\right)(t)\right\| \leq K_O\|P - \widehat{P}\|, \text{ where } K_L = \|(\mu + \delta)\|$$

This shows that, for $\mathbf{A}\left(L_1, M_1, N_{1,} O_1\right)$, we have.

$$\left\|\mathbf{A}(\mathcal{S}, \mathcal{V}, \mathcal{I}, P)(t) - \mathbf{A}\left(\widehat{\mathcal{S}}, \widehat{\mathcal{V}}, \hat{\mathcal{I}}, \widehat{P}\right)(t)\right\| = \frac{1-\eta}{M(\eta)}\max_{\mathrm{t}\in[0,\mathrm{T}]}\left|(\mathcal{S}, \mathcal{V}, \mathcal{I}, P(t) - \left(\widehat{\mathcal{S}}, \widehat{\mathcal{V}}, \hat{\mathcal{I}}, \widehat{P}\right)(t)\right|$$

$$\leq \frac{1-\eta}{M(\eta)}\left\|(\mathcal{S}, \mathcal{V}, \mathcal{I}, P) - \left(\widehat{\mathcal{S}}, \widehat{\mathcal{V}}, \hat{\mathcal{I}}, \widehat{P}\right)\right\|$$

$$\leq \frac{1-\eta}{M(\eta)}\mathbf{K}$$

with $\mathbf{K} = \max\{K_L, K_M, K_N, K_O\} < 1$ is Lipschitzian constant.

$$\Rightarrow \mathbf{A}(\mathcal{S}, \mathcal{V}, \mathcal{I}, P) \text{ is a non - expansive map.}$$

To prove $\mathbf{B}(L_2, M_2, N_2, O_2)$ is compact and continuous:

Let us assume the modulus of all continuous operators L,M,N,O, defined in (8) are positively bounded with constants $\mathfrak{C}_L, \mathfrak{C}_M, \mathfrak{C}_N, \mathfrak{C}_O, \mathfrak{D}_L, \mathfrak{D}_M, \mathfrak{D}_N, \mathfrak{D}_O$ satisfying,

$$|L(t, \mathcal{S})| \leq \mathfrak{C}_L\|\mathcal{S}\| + \mathfrak{D}_L$$
$$|M(t, \mathcal{V})| \leq \mathfrak{C}_M\|\mathcal{V}\| + \mathfrak{D}_M$$
$$|N(t, \mathcal{I})| \leq \mathfrak{C}_N\|\mathcal{I}\| + \mathfrak{D}_N$$
$$|O(t, P)| \leq \mathfrak{C}_O\|P\| + \mathfrak{D}_O$$

Let us consider a closed subset $\mathbf{B}$ of Z as $\mathbf{B} = \{(\mathcal{S}, \mathcal{V}, \mathcal{I}, P) \in \mathrm{Z} / \|(\mathcal{S}, \mathcal{V}, \mathcal{I}, P)\| \leq \Lambda, \Lambda > 0\}$.

For $(\mathcal{S}, \mathcal{V}, \mathcal{I}, P) \in \mathbf{B}$, we have,

$$\Rightarrow \|L_2(t, \mathcal{S})\| = \max_{t\in[0,T]} \left| \frac{\eta}{M(\eta)\Gamma\eta} \int_0^t (t-y)^{\eta-1} \mathrm{L}(y, \mathcal{S}(y))\mathrm{dy} \right|$$
$$\leq \frac{\xi^\eta}{M(\eta)\Gamma\eta} \int_0^\xi (\xi - y)^{\eta-1} |L(y, \mathcal{S}(y))|\mathrm{dy}$$
$$\leq \frac{\xi^\eta}{M(\eta)\Gamma\eta} \mathfrak{C}_L \Lambda + \mathfrak{O}_L$$

In the same way, we have

$$\|M_2(t, \mathcal{V})\| \leq \frac{\mathfrak{C}_M \Lambda + \mathfrak{O}_M}{M(\eta)\Gamma\eta}, \|N_2(t, \mathcal{I})\| \leq \frac{\mathfrak{C}_N \Lambda + \mathfrak{O}_N}{M(\eta)\Gamma\eta}, \|O_2(t, P)\| \leq \frac{\mathfrak{C}_O \Lambda + \mathfrak{O}_O}{M(\eta)\Gamma\eta}$$

Now let us derive the maximum norm of $\|\mathbf{B}(L_2, M_2, N_2, O_2)\|$ as,

$\|\mathbf{B}(L_2, M_2, N_2, O_2)\| = \leq \frac{\xi^\eta}{M(\eta)\Gamma\eta}\left[(\mathfrak{C}_L + \mathfrak{C}_M + \mathfrak{C}_N + \mathfrak{C}_O)\Lambda + \mathfrak{O}_L + \mathfrak{O}_M + \mathfrak{O}_N + \mathfrak{O}_O\right] =$ £, a positive constant.

Hence, $\|\mathbf{B}(\mathcal{S}, \mathcal{V}, \mathcal{I}, P)\| \leq$ £ $\Rightarrow \mathbf{B}$ is an uniformly bounded operator.

For $t_1 < t_2 \in [0, T]$, we have.

To prove $\mathbf{B}$ is equi-continuous for $t_1 < t_2 \in [0, T]$.

$$|L_2(t_2, \mathcal{S}) - L_2(t_1, \mathcal{S})|$$
$$= \frac{\eta}{M(\eta)\Gamma\eta} \left| \int_0^{t_2} (t-y)^{\eta-1} \mathrm{L}(y, \mathcal{S}(y))\mathrm{dy} - \int_0^{t_1} (t-y)^{\eta-1} \mathrm{L}(y, \mathcal{S}(y))\mathrm{dy} \right|$$
$$\leq \frac{\eta}{M(\eta)\Gamma\eta} \left(\int_0^{t_2} (t-y)^{\eta-1} - \int_0^{t_1} (t-y)^{\eta-1} \right) [(\mathfrak{C}_L)\Lambda + \mathfrak{O}_L]$$
$$\leq \frac{(\mathfrak{C}_L)\Lambda + \mathfrak{O}_L}{M(\eta)\Gamma\eta} \left(t_2^\eta - t_1^\eta\right) \tag{14}$$

Also for M_2, N_2, O_2 satisfies inequality in (14),

$$|M_2(t_2, \mathcal{V}) - M_2(t_1, \mathcal{V})| \leq \frac{(\mathfrak{C}_M)\Lambda + \mathfrak{O}_M}{M(\eta)\Gamma\eta} \left(t_2^\eta - t_1^\eta\right)$$
$$|N_2(t_2, \mathcal{I}) - N_2(t_1, \mathcal{I})| \leq \frac{(\mathfrak{C}_N)\Lambda + \mathfrak{O}_N}{M(\eta)\Gamma\eta} \left(t_2^\eta - t_1^\eta\right)$$
$$|O_2(t_2, P) - O_2(t_1, P)| \leq \frac{(\mathfrak{C}_O)\Lambda + \mathfrak{O}_O}{M(\eta)\Gamma\eta} \left(t_2^\eta - t_1^\eta\right)$$

$\Rightarrow \|\mathbf{B}(L_2, M_2, N_2, O_2)(t_2) - \mathbf{B}(L_2, M_2, N_2, O_2)(t_1)\| \to 0$, as $t_1 \to t_2$ independent of the operators $(\mathcal{S}, \mathcal{V}, \mathcal{I}, P)$.

$\Rightarrow \mathbf{B}(L_2, M_2, N_2, O_2)$ is an operator of equi-continuity, which is also completely continuous.

By Arzela's theorem, uniformly boundedness postulate of a completely continuous map is relatively compact. Contraction and continuity of the operators **A** and **B** imposes the single solution existence according to theorem of fixed point by Krasnoselski.

Theorem 4.5.2 Attractive solution *The postulate* $(\nVdash_1)$ *signifies our COVID 19 mathematical model* (1) *has an*

(i) *unique result if* $\frac{\xi^\eta}{M(\eta)\Gamma\eta}\mathrm{K} < 1$, *where* $\mathbf{K} = \max\{K_L, K_M, K_N, K_O\}$
(ii) *attractive solution if trivial solution* $\varphi(\mathrm{t}) = 0$ *such that* $\|x_0\| \leq \varepsilon, \Rightarrow \lim_{t\to\infty} x_0 = 0$.

Proof Let us define an operator $\mathrm{W} = (W_1, W_2, W_3, W_4)$: $\mathrm{Z} \to \mathrm{Z}$ using (9) as follows,

$$\left.\begin{aligned}
W_1(\mathcal{S},\mathcal{V},\mathcal{I},P)(t) &= \mathcal{S}_0 + \tfrac{1-\eta}{M(\eta)}\,\mathrm{L}(t,\mathcal{S}(t)) + \tfrac{\eta}{M(\eta)\Gamma\eta}\int_0^t (t-y)^{\eta-1}\mathrm{L}(\mathrm{y},\mathcal{S}(\mathrm{y}))\mathrm{dy}\\
W_2(\mathcal{S},\mathcal{V},\mathcal{I},P)(t) &= \mathcal{V}_0 + \tfrac{1-\eta}{M(\eta)}M(t,\mathcal{V}(t)) + \tfrac{\eta}{M(\eta)\Gamma\eta}\int_0^t (t-y)^{\eta-1}M(y,\mathcal{V}(y))dy\\
W_3(\mathcal{S},\mathcal{V},\mathcal{I},P)(t) &= \mathcal{I}_0 + \tfrac{1-\eta}{M(\eta)}\,\mathrm{N}(t,\mathcal{I}(t)) + \tfrac{\eta}{M(\eta)\Gamma\eta}\int_0^t (t-y)^{\eta-1}\mathrm{N}(\mathrm{y},\mathcal{I}(\mathrm{y}))\mathrm{dy}\\
W_4(\mathcal{S},\mathcal{V},\mathcal{I},P)(t) &= P_0 + \tfrac{1-\eta}{M(\eta)}\,\mathrm{O}(t,P(t)) + \tfrac{\eta}{M(\eta)\Gamma\eta}\int_0^t (t-y)^{\eta-1}\mathrm{O}(\mathrm{y},P(\mathrm{y}))\,\mathrm{dy}
\end{aligned}\right\} \quad (15)$$

Accordingly for $(\mathcal{S},\mathcal{V},\mathcal{I},P)$, $(\widehat{\mathcal{S}},\widehat{\mathcal{V}},\widehat{\mathcal{I}},\widehat{P}) \in \mathrm{Z}$, and using (10) we claim,

$$\left\|W_1(\mathcal{S},\mathcal{V},\mathcal{I},P)(t) - W_1\left(\widehat{\mathcal{S}},\widehat{\mathcal{V}},\hat{\mathcal{I}},\widehat{P}\right)(t)\right\| = \frac{1-\eta}{M(\eta)}\left\|\mathrm{L}(t,\mathcal{S}(t)) - \mathrm{L}\left(t,\hat{\mathcal{S}}(t)\right)\right\|$$

$$+ \frac{\eta}{M(\eta)\Gamma\eta}\int_0^t \left\|\mathrm{L}(\mathrm{y},\mathcal{S}(\mathrm{y})) - \mathrm{L}\left(\mathrm{y},\hat{\mathcal{S}}(\mathrm{y})\right)\right\|(t-y)^{\eta-1}\mathrm{L}(\mathrm{y},\mathcal{S}(\mathrm{y}))\mathrm{dy}$$

$$\left\|W_1(\mathcal{S},\mathcal{V},\mathcal{I},P)(t) - W_1\left(\widehat{\mathcal{S}},\widehat{\mathcal{V}},\hat{\mathcal{I}},\widehat{P}\right)(t)\right\| \leq \frac{1-\eta}{M(\eta)}K_L\left\|\mathcal{S}-\hat{\mathcal{S}}\right\| + \frac{\xi^\eta}{M(\eta)\Gamma\eta}K_L\left\|\mathcal{S}-\hat{\mathcal{S}}\right\|$$

$$\leq \left(\frac{1-\eta}{M(\eta)} + \frac{\xi^\eta}{M(\eta)\Gamma\eta}\right)K_L\left\|\mathcal{S}-\hat{\mathcal{S}}\right\|$$

As $\mathcal{S}(t) \to \hat{\mathcal{S}}(t)$ then $\left\|\mathcal{S}-\hat{\mathcal{S}}\right\| \to 0$, the above inequality becomes,

$$\left\|W_1(\mathcal{S},\mathcal{V},\mathcal{I},P)(t) - W_1\left(\widehat{\mathcal{S}},\widehat{\mathcal{V}},\hat{\mathcal{I}},\widehat{P}\right)(t)\right\| \leq \left(\frac{1-\eta}{M(\eta)} + \frac{\xi^\eta}{M(\eta)\Gamma\eta}\right)K_L \leq 1,$$

with

$$\left\|W_1(\mathcal{S},\mathcal{V},\mathcal{I},P)(t) - W_1\left(\widehat{\mathcal{S}},\widehat{\mathcal{V}},\hat{\mathcal{I}},\widehat{P}\right)(t)\right\|\left(1 - \left(\frac{1-\eta}{M(\eta)} + \frac{\xi^\eta}{M(\eta)\Gamma\eta}\right)K_L\right) \leq 0$$

Proceeding in the same way, we have

$$\left\|W_2(\mathcal{S},\mathcal{V},\mathcal{I},P)(t) - W_2\left(\widehat{S},\widehat{V},\hat{\mathcal{I}},\hat{P}\right)(t)\right\|\left(1 - \left(\frac{1-\eta}{M(\eta)} + \frac{\xi^\eta}{M(\eta)\Gamma\eta}\right)K_M\right) \leq 0$$

$$\left\|W_3(\mathcal{S},\mathcal{V},\mathcal{I},P)(t) - W_3\left(\widehat{S},\widehat{V},\hat{\mathcal{I}},\hat{P}\right)(t)\right\|\left(1 - \left(\frac{1-\eta}{M(\eta)} + \frac{\xi^\eta}{M(\eta)\Gamma\eta}\right)K_N\right) \leq 0$$

$$\left\|W_4(\mathcal{S},\mathcal{V},\mathcal{I},P)(t) - W_4\left(\widehat{S},\widehat{V},\hat{\mathcal{I}},\hat{P}\right)(t)\right\|\left(1 - \left(\frac{1-\eta}{M(\eta)} + \frac{\xi^\eta}{M(\eta)\Gamma\eta}\right)K_O\right) \leq 0$$

Hence the operator

$$\left\|\mathrm{W}(\mathcal{S},\mathcal{V},\mathcal{I},P)-\mathrm{W}\left(\widehat{\mathcal{S}},\widehat{\mathcal{V}},\hat{\mathcal{I}},\widehat{P}\right)\right\| \leq \left(\frac{1-\eta}{M(\eta)}+\frac{\xi^{\eta}}{M(\eta)\Gamma\eta}\right)\mathbf{K}\left[\left\|(\mathcal{S},\mathcal{V},\mathcal{I},P)-\left(\widehat{\mathcal{S}},\widehat{\mathcal{V}},\hat{\mathcal{I}},\widehat{P}\right)\right\|\right] \tag{16}$$

$\Rightarrow$ The contraction map W inherits the properties of Schauder's and Krasnoselski's theorem on unique fixed point.

Thus the unique solution is exhibited for system (5).

Attractivity of the derived solution

The unique solution is attractive if the zero solution $(\mathcal{S},\mathcal{V},\mathcal{I},P)(t)=0$ such that

$$\|(\mathcal{S},\mathcal{V},\mathcal{I},P)\| \leq \varepsilon, \Rightarrow \lim_{t\to\infty}(\mathcal{S},\mathcal{V},\mathcal{I},P)(t)=0. \tag{17}$$

Also the solution is attractive if the trivial solution $\varphi(t)=0$ such that $x_0 \leq \varepsilon$,

$\Rightarrow \lim_{t\to\infty} x_0 = 0$.

$\Rightarrow$ Asymptotically stable.

Hyer-Ulam's stability

Stability of the solution to modelled fractional differential equation system in Hyer-Ulam's style is studied with differential inequality [52].

Theorem *The unique solution* $(\mathcal{S},\mathcal{V},\mathcal{I},P)$ *of the model* (1) *is stable of Hyer-Ulam's kind* [45] *if the spectral radius of* $\begin{pmatrix} \mathfrak{l} & \mathfrak{l} & \mathfrak{l} & \mathfrak{l} \\ \mathfrak{m} & \mathfrak{m} & \mathfrak{m} & \mathfrak{m} \\ \mathfrak{n} & \mathfrak{n} & \mathfrak{n} & \mathfrak{n} \\ \mathfrak{o} & \mathfrak{o} & \mathfrak{o} & \mathfrak{o} \end{pmatrix}$ *lies strictly inside the unit circle (discrete dichotomy)* [50] *given by* $|\mathfrak{l}+\mathfrak{m}+\mathfrak{n}+\mathfrak{o}|<1$. *where,*

$$\mathfrak{l}=\left(\frac{1-\eta}{M(\eta)}+\frac{\xi^{\eta}}{M(\eta)\Gamma\eta}\right)K_L;\quad \mathfrak{m}=\left(\frac{1-\eta}{M(\eta)}+\frac{\xi^{\eta}}{M(\eta)\Gamma\eta}\right)K_M;$$
$$\mathfrak{n}=\left(\frac{1-\eta}{M(\eta)}+\frac{\xi^{\eta}}{M(\eta)\Gamma\eta}\right)K_N;\quad \mathfrak{o}=\left(\frac{1-\eta}{M(\eta)}+\frac{\xi^{\eta}}{M(\eta)\Gamma\eta}\right)K_O$$

Proof The system defined in model (5) has an unique solution by theorem.

To its contrary. let $(\mathcal{S},\mathcal{V},\mathcal{I},P)$ and $\left(\widehat{\mathcal{S}},\widehat{V},\hat{\mathcal{I}},\hat{P}\right)$ be two different solutions of the same model,then we write with help of (16)

$$\begin{aligned}
&\left\|\mathrm{W}(\mathcal{S},\mathcal{V},\mathcal{I},P)-\mathrm{W}\left(\widehat{\mathcal{S}},\widehat{\mathcal{V}},\hat{\mathcal{I}},\widehat{P}\right)\right\| \\
&\leq \left(\frac{1-\eta}{M(\eta)}+\frac{\xi^{\eta}}{M(\eta)\Gamma\eta}\right)\mathbf{K}\left[\left\|(\mathcal{S},\mathcal{V},\mathcal{I},P)-\left(\widehat{\mathcal{S}},\widehat{\mathcal{V}},\hat{\mathcal{I}},\widehat{P}\right)\right\|\right] \\
&= \left(\frac{1-\eta}{M(\eta)}+\frac{\xi^{\eta}}{M(\eta)\Gamma\eta}\right)K_L\left\|\mathcal{S}-\hat{\mathcal{S}}\right\|+\left(\frac{1-\eta}{M(\eta)}+\frac{\xi^{\eta}}{M(\eta)\Gamma\eta}\right)K_M\left\|\mathcal{V}-\hat{\mathcal{V}}\right\| \\
&\quad+\left(\frac{1-\eta}{M(\eta)}+\frac{\xi^{\eta}}{M(\eta)\Gamma\eta}\right)K_N\left\|\mathcal{I}-\hat{\mathcal{I}}\right\|+\left(\frac{1-\eta}{M(\eta)}+\frac{\xi^{\eta}}{M(\eta)\Gamma\eta}\right)K_O\left\|P-\widehat{P}\right\|
\end{aligned} \tag{18}$$

Linearization of above norm for $(\mathcal{S},\mathcal{V},\mathcal{I},P)$ and $\left(\widehat{\mathcal{S}},\widehat{V},\hat{\mathcal{I}},\hat{P}\right)$ in terms of matrices, we have

$$\left\|(\mathcal{S},\mathcal{V},\mathcal{I},P)-\left(\widehat{\mathcal{S}},\widehat{\mathcal{V}},\hat{\mathcal{I}},\widehat{P}\right)\right\| \leq \begin{vmatrix} \mathfrak{l} & \mathfrak{l} & \mathfrak{l} & \mathfrak{l} \\ \mathfrak{m} & \mathfrak{m} & \mathfrak{m} & \mathfrak{m} \\ \mathfrak{n} & \mathfrak{n} & \mathfrak{n} & \mathfrak{n} \\ \mathfrak{o} & \mathfrak{o} & \mathfrak{o} & \mathfrak{o} \end{vmatrix} \begin{pmatrix} \left\|\mathcal{S}-\hat{\mathcal{S}}\right\| \\ \left\|\mathcal{V}-\hat{\mathcal{V}}\right\| \\ \left\|\mathcal{I}-\hat{\mathcal{I}}\right\| \\ \left\|P-\widehat{P}\right\| \end{pmatrix}$$ converges to zero, with $\mathfrak{l},\mathfrak{m},\mathfrak{n},\mathfrak{o}$ defined above.

The characteristic roots of the above matrix are $x_1 = 0, x_2 = 0, x_3 = 0, x_4 = \mathfrak{l} + \mathfrak{m} + \mathfrak{n} + \mathfrak{o}$.

The spectral radius denoted by $r = \max\{|x_i|, i = 1, 2, 3, 4\} < 1$ exhibits a discrete dichotomy making the solution of model (1) as Ulam Hyer's stable.

Numerical Method and Results

In this section, numerical algorithm for the designed model (1) is derived using Adams Bashforth technique [31].

Applying Lagrange's interpolation formula to our ABC fractional order model governing kernels in (9) and iterate as,

$$\mathcal{S}(t)-\mathcal{S}(0)-\frac{1-\eta}{M(\eta)}\mathrm{L}(t,\mathcal{S}(t))=\frac{\eta}{M(\eta)\Gamma\eta}\int_0^t (t-y)^{\eta-1}L(y,\mathcal{S}(y))\,\mathrm{d}y \tag{19}$$

Step 1.

Setting $t = t_{\acute{\upsilon}+1}$, for $\acute{\upsilon} = 0, 1, 2\ldots$

$$\begin{aligned}\mathcal{S}(t_{\acute{\upsilon}+1})-\mathcal{S}(0)-\frac{1-\eta}{M(\eta)}\mathrm{L}(t_{\acute{\upsilon}},\mathcal{S}(t_{\acute{\upsilon}})) &= \frac{\eta}{M(\eta)\Gamma\eta}\int_0^{t_{\acute{\upsilon}+1}}(t_{\acute{\upsilon}+1}-y)^{\eta-1}\mathrm{L}(\mathrm{y},\mathcal{S}(\mathrm{y}))\,\mathrm{dy}\\ &= \frac{\eta}{M(\eta)\Gamma\eta}\sum_{\acute{\omega}=0}^{\acute{\upsilon}}\int_{t_{\acute{\omega}}}^{t_{\acute{\omega}+1}}(t_{\acute{\upsilon}+1}-y)^{\eta-1}\mathrm{L}(\mathrm{y},\mathcal{S}(\mathrm{y}))\,\mathrm{dy}.\end{aligned} \tag{20}$$

Step 2.

Interpolating the function $\mathrm{L}(t,\mathcal{S}(t))$ on $[t_{\acute{\omega}}, t_{\acute{\omega}+1}]$ we get,

$$\mathrm{L}(\mathrm{y},\mathcal{S}(t))\cong\frac{L(t_{\acute{\omega}},\mathcal{S}(t_{\acute{\omega}}))}{\delta}\left(t-t_{\acute{\omega}-1}\right)+\frac{L\left(t_{\acute{\omega}-1,},\mathcal{S}\left(t_{\acute{\omega}-1}\right)\right)}{\delta}(t-t_{\acute{\omega}}) \tag{21}$$

Step 3.

Applying this interpolated result on the susceptible group $\mathcal{S}(t)$,

$$\begin{aligned}&\mathcal{S}\left(t_{\acute{\upsilon}+1}\right)-\mathcal{S}(0)-\frac{1-\eta}{M(\eta)}\mathrm{L}(t_{\acute{\upsilon}},\mathcal{S}(t_{\acute{\upsilon}})=\frac{\eta}{M(\eta)\Gamma\eta}\\ &\sum_{\acute{\omega}=0}^{\acute{\upsilon}}\left(\frac{\mathrm{L}(t_{\acute{\omega}},\mathcal{S}(t_{\acute{\omega}}))}{\delta}\int_{t_{\acute{\omega}}}^{t_{\acute{\omega}+1}}(t-t_{\acute{\omega}-1})(t_{\acute{\upsilon}+1}-t)^{\eta-1}-\frac{\mathrm{L}(t_{\acute{\omega}-1},\mathcal{S}(t_{\acute{\omega}-1}))}{\delta}\int_{t_{\acute{\omega}}}^{t_{\acute{\omega}+1}}(t-t_{\acute{\omega}})(t_{\acute{\upsilon}+1}-t)^{\eta-1}dt\right)\\ &=\frac{\eta}{M(\eta)\Gamma\eta}\sum_{\acute{\omega}=0}^{\acute{\upsilon}}\left(\frac{\mathrm{L}(t_{\acute{\omega}},\mathcal{S}(t_{\acute{\omega}}))}{\delta}A_{\acute{\omega}-1,\eta}-\frac{\mathrm{L}(t_{\acute{\omega}-1},\mathcal{S}(t_{\acute{\omega}-1}))}{\delta}A_{\acute{\omega},\eta}\right)\end{aligned} \tag{22}$$

Step 4.

Computing the auxiliary functions $A_{\acute{\omega}-1,\eta}$, $A_{\acute{\omega},\eta}$ describing the discretization of values for $\acute{\omega} = 0$ to $\acute{\upsilon}$.

$$\begin{aligned} A_{\acute{\omega}-1,\eta} &= \int_{t_{\acute{\omega}}}^{t_{\acute{\omega}+1}} \big(t - t_{\acute{\omega}-1}\big)(t_{\acute{\upsilon}+1} - t)^{\eta-1}\mathrm{d}t \\ &= -\left\{ \begin{array}{c} \frac{1}{\eta}\big[\big(t_{\acute{\omega}+1} - t_{\acute{\omega}-1}\big)(t_{\acute{\upsilon}+1} - t_{\acute{\omega}+1})^{\eta} - \big(t_{\acute{\omega}} - t_{\acute{\omega}-1}\big)(t_{\acute{\upsilon}+1} - t_{\acute{\omega}})^{\eta}\big] \\ +\frac{1}{\eta(\eta+1)}\big[(t_{\acute{\upsilon}+1} - t_{\acute{\omega}+1})^{\eta+1} - (t_{\acute{\upsilon}+1} - t_{\acute{\omega}})^{\eta+1}\big] \end{array} \right\} \end{aligned} \tag{23}$$

$$\begin{aligned} A_{\acute{\omega},\eta} &= \int_{t_{\acute{\omega}}}^{t_{\acute{\omega}+1}} (t - t_{\acute{\omega}})(t_{\acute{\upsilon}+1} - t)^{\eta-1}dt \\ &= -\left\{ \frac{1}{\eta}\big[(t_{\acute{\omega}+1} - t_{\acute{\omega}})(t_{\acute{\upsilon}+1} - t_{\acute{\omega}+1})^{\eta}\big] + \frac{1}{\eta(\eta+1)}\big[(t_{\acute{\upsilon}+1} - t_{\acute{\omega}+1})^{\eta+1} - (t_{\acute{\upsilon}+1} - t_{\acute{\omega}})^{\eta+1}\big] \right\} \end{aligned} \tag{24}$$

Substituting $t_{\acute{\omega}} = \acute{\omega}\delta$ in (23), (24) then we have,

$$\begin{aligned} A_{\acute{\omega}-1,\eta} &= -\frac{\delta^{\eta+1}}{\eta}\left[\begin{array}{c} \big(\acute{\omega}+1-\big(\acute{\omega}-1\big)\big)\big(\acute{\upsilon}+1-\big(\acute{\omega}+1\big)\big)^{\eta} \\ -\big(\acute{\omega}-\big(\acute{\omega}-1\big)\big)\big(\acute{\upsilon}+1-\acute{\omega}\big)^{\eta} \end{array} \right] \\ &\quad - \frac{\delta^{\eta+1}}{\eta(\eta+1)}\Big[\big(\acute{\upsilon}+1-\big(\acute{\omega}+1\big)\big)^{\eta+1} - \big(\acute{\upsilon}+1-\acute{\omega}\big)^{\eta+1}\Big] \\ &= \frac{\delta^{\eta+1}}{\eta}\left[\begin{array}{c} -2(\eta+1)\big(\acute{\upsilon}-\acute{\omega}\big)^{\eta} + (\eta+1)\big(\acute{\upsilon}+1-\acute{\omega}\big)^{\eta} \\ -\big(\acute{\upsilon}-\acute{\omega}\big)^{\eta+1} + \big(\acute{\upsilon}+1-\acute{\omega}\big)^{\eta+1} \end{array} \right] \\ &= \frac{\delta^{\eta+1}}{\eta(\eta+1)}\left[\begin{array}{c} \big(\acute{\upsilon}-\acute{\omega}\big)^{\eta}\big(-2\big(\acute{\omega}+1\big) - \big(\acute{\upsilon}-\acute{\omega}\big)\big) \\ +\big(\acute{\upsilon}+1-\acute{\omega}\big)^{\eta}\big(\eta+1+\acute{\upsilon}+1-\acute{\omega}\big) \end{array} \right] \\ &= \frac{\delta^{\eta+1}}{\eta(\eta+1)}\big[\big(\acute{\upsilon}+1-\acute{\omega}\big)^{\eta}\big(\acute{\upsilon}-\acute{\omega}+2+\eta\big) - \big(\acute{\upsilon}-\acute{\omega}\big)^{\eta}\big(\acute{\upsilon}-\acute{\omega}+2+2\eta\big)\big] \end{aligned} \tag{25}$$

$$\begin{aligned} A_{\acute{\omega},\eta} &= \frac{-\delta^{\eta+1}}{\eta}\left\{ \begin{array}{c} \big[\big(\acute{\upsilon}+1-\acute{\omega}\big)\big(\acute{\upsilon}+1-\big(\acute{\omega}+1\big)\big)^{\eta}\big]+ \\ \frac{1}{(\eta+1)}\Big[\big(\acute{\upsilon}+1-\big(\acute{\omega}+1\big)\big)^{\eta+1} - \big(\acute{\upsilon}+1-\acute{\omega}\big)^{\eta+1}\Big] \end{array} \right\} \\ &= \frac{\delta^{\eta+1}}{\eta(\eta+1)}\Big[-(\eta+1)\big(\acute{\upsilon}-\acute{\omega}\big)^{\eta} - \big(\acute{\upsilon}-\acute{\omega}\big)^{\eta+1} + \big(\acute{\upsilon}+1-\acute{\omega}\big)^{\eta+1}\Big] \\ &= \frac{\delta^{\eta+1}}{\eta(\eta+1)}\Big[\big(\acute{\upsilon}-\acute{\omega}\big)^{\eta}\big(-(\eta+1) - \big(\acute{\upsilon}-\acute{\omega}\big)\big) + \big(\acute{\upsilon}+1-\acute{\omega}\big)^{\eta+1}\Big] \\ &= \frac{\delta^{\eta+1}}{\eta(\eta+1)}\Big[\big(\acute{\upsilon}+1-\acute{\omega}\big)^{\eta+1} - \big(\acute{\upsilon}-\acute{\omega}\big)^{\eta}\big(\acute{\upsilon}-\acute{\omega}+1+\eta\big)\Big] \end{aligned} \tag{26}$$

Step 5.

To derive the recurrence relation for all the equations in model (5)

Substituting (25) and (26) in (22), we have the following equations

$$\mathcal{S}(t_{\acute{\upsilon}+1}) - \mathcal{S}(0) - \frac{1-\eta}{M(\eta)}\mathrm{L}(t_{\acute{\upsilon}}, \mathcal{S}(t_{\acute{\upsilon}})) = \frac{\eta}{M(\eta)\Gamma\eta}\sum_{\acute{\omega}=0}^{\acute{\upsilon}}\left(\begin{array}{l}\frac{\mathrm{L}(t_{\acute{\omega}},\mathcal{S}(t_{\acute{\omega}}))}{\Gamma\eta+2}\delta^{\eta}\left[(\acute{\upsilon}+1-\acute{\omega})^{\eta}(\acute{\upsilon}-\acute{\omega}+2+\eta)-(\acute{\upsilon}-\acute{\omega})^{\eta}(\acute{\upsilon}-\acute{\omega}+2+2\eta)\right]\\ -\frac{\mathrm{L}(t_{\acute{\omega}-1},\mathcal{S}(t_{\acute{\omega}-1}))}{\Gamma\eta+2}\delta^{\eta}\left[(\acute{\upsilon}+1-\acute{\omega})^{\eta+1}-(\acute{\upsilon}-\acute{\omega})^{\eta}(\acute{\upsilon}-\acute{\omega}+1+\eta)\right]\end{array}\right) \tag{27}$$

$$\mathcal{V}(t_{\acute{\upsilon}+1}) - \mathcal{V}(0) - \frac{1-\eta}{M(\eta)}\mathrm{M}(t_{\acute{\upsilon}}, \mathcal{V}(t_{\acute{\upsilon}})) = \frac{\eta}{M(\eta)\Gamma\eta}\sum_{\acute{\omega}=0}^{\acute{\upsilon}}\left(\begin{array}{l}\frac{\mathrm{M}(t_{\acute{\omega}},\mathcal{V}(t_{\acute{\omega}}))}{\Gamma\eta+2}\delta^{\eta}\left[(\acute{\upsilon}+1-\acute{\omega})^{\eta}(\acute{\upsilon}-\acute{\omega}+2+\eta)-(\acute{\upsilon}-\acute{\omega})^{\eta}(\acute{\upsilon}-\acute{\omega}+2+2\eta)\right]\\ -\frac{\mathrm{M}(t_{\acute{\omega}-1},\mathcal{V}(t_{\acute{\omega}-1}))}{\Gamma\eta+2}\delta^{\eta}\left[(\acute{\upsilon}+1-\acute{\omega})^{\eta+1}-(\acute{\upsilon}-\acute{\omega})^{\eta}(\acute{\upsilon}-\acute{\omega}+1+\eta)\right]\end{array}\right) \tag{28}$$

$$\mathcal{I}(t_{\acute{\upsilon}+1}) - \mathcal{I}(0) - \frac{1-\eta}{M(\eta)}\mathrm{N}(t_{\acute{\upsilon}}, \mathcal{I}(t_{\acute{\upsilon}})) = \frac{\eta}{M(\eta)\Gamma\eta}\sum_{\acute{\omega}=0}^{\acute{\upsilon}}\left(\begin{array}{l}\frac{\mathrm{N}(t_{\acute{\omega}},\mathcal{I}(t_{\acute{\omega}}))}{\Gamma\eta+2}\delta^{\eta}\left[(\acute{\upsilon}+1-\acute{\omega})^{\eta}(\acute{\upsilon}-\acute{\omega}+2+\eta)-(\acute{\upsilon}-\acute{\omega})^{\eta}(\acute{\upsilon}-\acute{\omega}+2+2\eta)\right]\\ -\frac{\mathrm{N}(t_{\acute{\omega}-1},\mathcal{I}(t_{\acute{\omega}-1}))}{\Gamma\eta+2}\delta^{\eta}\left[(\acute{\upsilon}+1-\acute{\omega})^{\eta+1}-(\acute{\upsilon}-\acute{\omega})^{\eta}(\acute{\upsilon}-\acute{\omega}+1+\eta)\right]\end{array}\right) \tag{29}$$

$$P(t_{\acute{\upsilon}+1}) - P(0) - \frac{1-\eta}{M(\eta)}\mathrm{O}(t_{\acute{\upsilon}}, P(t_{\acute{\upsilon}})) = \frac{\eta}{M(\eta)\Gamma\eta}\sum_{\acute{\omega}=0}^{\acute{\upsilon}}\left(\begin{array}{l}\frac{\mathrm{O}(t_{\acute{\omega}},P(t_{\acute{\omega}}))}{\Gamma\eta+2}\delta^{\eta}\left[(\acute{\upsilon}+1-\acute{\omega})^{\eta}(\acute{\upsilon}-\acute{\omega}+2+\eta)-(\acute{\upsilon}-\acute{\omega})^{\eta}(\acute{\upsilon}-\acute{\omega}+2+2\eta)\right]\\ -\frac{\mathrm{O}(t_{\acute{\omega}-1},\mathrm{P}(t_{\acute{\omega}-1}))}{\Gamma\eta+2}\delta^{\eta}\left[(\acute{\upsilon}+1-\acute{\omega})^{\eta+1}-(\acute{\upsilon}-\acute{\omega})^{\eta}(\acute{\upsilon}-\acute{\omega}+1+\eta)\right]\end{array}\right) \tag{30}$$

Equations (27)–(30) offer the numerical analysis to our model contemplated in (5).

Results and Discussion

The graphical visualisation of the solution for the model (5) is analysed with the numerical input of the data tabulated below. The data have been collected from Our World In Data [51] source of COVID-19 reported for India.

Numerical Simulations: Reduced Incidence Rates with Vaccination

The impact of the variables defining the governing commensurate model equations on the transference and control of the pandemic disease is validated by stimulating for the reported real time data from OWID-Covid data [51]. The most minimal fractional order derivatives yields better approximate results proved by researchers exist in the literature [22–26, 28–31, 42–48]. In view of that point, the fractional iterations of very smallest order simulations were shown with $\eta = 0.02$ for declining transmission rate of susceptibles β(1211.03, 1000.00, 800.13) in Fig. 1. The susceptibles being contagious to the virus converges eventually after 120 days. The disease spread will be controlled by and by in the next 12 weeks quietly.

As the rate of vaccinated being infected $\alpha = 310.251, 200.123, 0$ reduces, the numerical derivation for most small arbitrary order $\eta = 0.02$ shown in different curves of Fig. 2, There arise a sudden increase of highly immuned vaccinated population $\mathcal{V}(t)$ due to the decay or

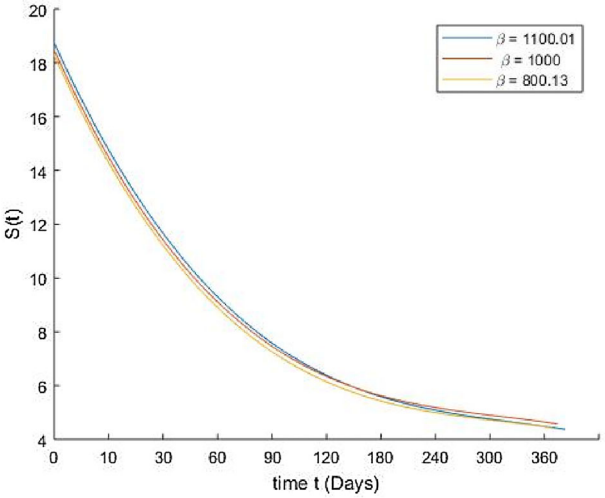

Fig. 1 The simulaton of susceptible individuals $\mathcal{S}(t)$ for a period of 360 days for various decreasing rate of susceptible infections β with order $\eta = 0.02$

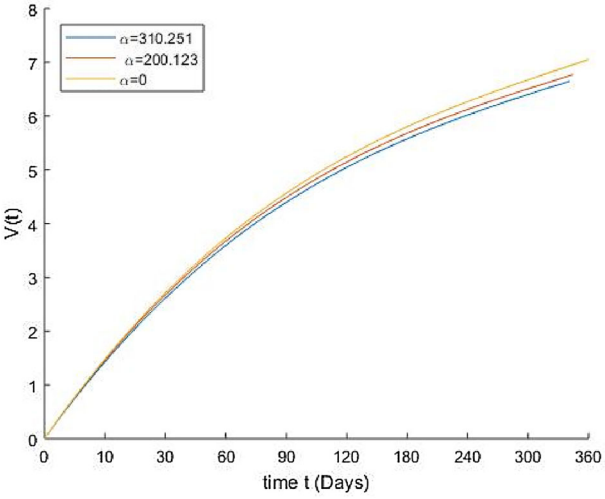

Fig. 2 The simulation of gradual increase of vaccinated population, $\mathcal{V}(t)$visualising gradual decrease of new infections for various rate of vaccinated infections α

avoidance of contact with infectious. Thus by decreasing the contact rate (β, α) of susceptibles and vaccinated people with infectious ones, the flow of curves predict the control of disease at the appropriate time. Self -hygiene and vaccination are the duo noteworthy control measures in concern. By increasing personal precautionary activities of every individual the pandemic spread will be flattened shortly. In Fig. 3, the graph analyses the rapid hike of protected population $P(t)$ with various upsurge of self-prevention value $\Psi =$ 0.0261, 0.051, 0.078, 1.

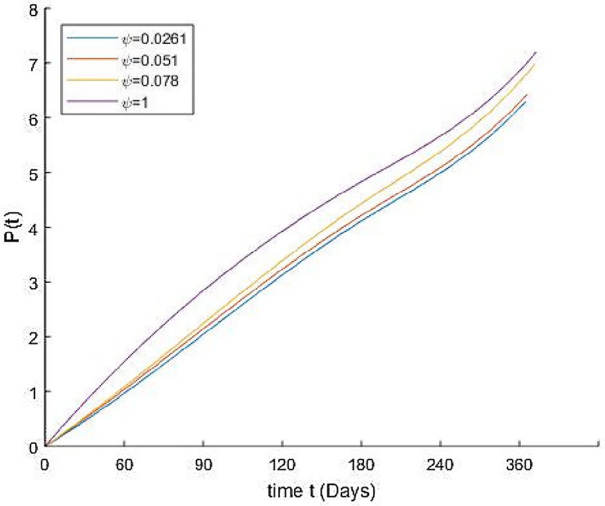

Fig. 3 The simulated results of protected population P(t) with improvised rate of various self preventive measures Ψ

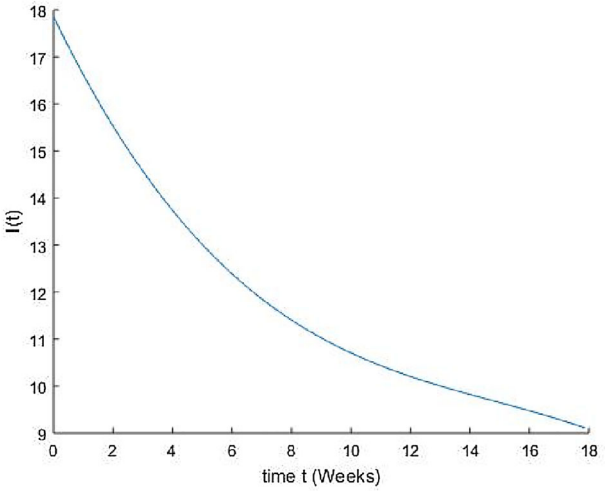

Fig. 4 The simulation of gradual decrease in infections $\mathcal{I}(t)$ due to rate of increase of self precautionary measures and decline in transmissions

The lower, the transmission rate and the most safeguard yields an imperceptible expansion of healthy people initiated gently.

The above Fig. 4 is graphed to embellish the distrainment of infected population $\mathcal{I}(t)$ for lesser carrying rates and death rates $\alpha = 100$, $\beta = 300$, $\delta = 0.0002$, $\mu = 0.00001$, $\phi = 0.00002$, $\gamma = 0.099$ by 18 weeks. The flow of infections started to reduce very rapidly shows the effective controllability of the disease to its nil infection state.

Conclusion

The COVID-19 fractional order $\mathcal{SVIP}$ model with multi control measures such as self- precautions and vaccination explores the flow of four groups susceptibles, vaccinated, infected people and protected ones in a contagious region. The proposed model have been framed and examined in terms of non-linear ABC type derivatives. The system possess two equilibrium points IFE and IPE. The infection free state IFE is locally asymptotic stable attracting close neighbourhood points iff $R_0 < 1$, whereas the disease continues persistently around IPE for $R_0 > 1$, inspite of vaccination and self-protection. The model has a single feasible solution is validated by theorems on fixed point and stability analysis of Hyer-Ulam's kind is performed. Semi-analytical method of Adam-Bashforth equations were derived for the proposed model. Transference of COVID-19 disease in India since the implementation of vaccination has been interrogated for real data recorded from Our World in data (OWID) web-link. Rapid vaccinations were implemented for the whole of our nation very expertly. Records of OWID evince that by vaccinating individuals help to build artificial immunity that defeats the worst severity of infections and reduce fatalities on the trot. The productive immunity of vaccine shots in triggering the inherited defence system of human cells is well-established in terms of Mittag–Leffler memory of ABC kernel function [46, 47]. The effect of mass vaccination and self-protective measures shown graphically conjectures the decline in infections' spread effectively in due course are studied with two views and listed below,

Minimised contact rates β, α and Efficient vaccination;

(i) Least-real order iterations of fractional differentiation for complex type systems provide pertinent results as desired [42–45] Hence fractional order graphs are simulated for the most minimal order $\eta = 0.02$.
(ii) Increased rate of vaccination 'v' results in decay of Susceptible population $\mathcal{S}(t)$ due to immigration of susceptible to vaccinated group $\mathcal{V}(t)$. The more, the vaccinated people causes the less in unvaccinated susceptibles.
(iii) By controlling the rate of susceptible people gets infected β, there is a decay of susceptible population $\mathcal{S}(t)$ to the equilibrium point on their respective paths slowly.
(iv) Due to relapse of vaccine efficiency, reducing the rate of vaccinated being infected α to 0, gradual hike in vaccinated population $\mathcal{V}(t)$ is attained.
(v) Maximal vaccination results in high immunity to fight against later infection and mortality.

Self-control strategy.

(i) Reduced transmission rates β, α and continuous immunization by vaccines result in a fast degradation of infected population $\mathcal{I}(t)$ reaching the infection free state IFE.
(ii) Self- precautionary measures Ψ shows effective result on reducing the virulent spread more effectively. As Ψ increases, the salubrious peaks of protected people $P(t)$ are visualised.

Acknowledgements All authors have read and approved this paper.

Funding No funds received.

Data Availability Not applicable.

Declarations

Conflict of interest The authors declare that they have no competing interest.financially and personally.

References

1. Data collected from http://covid19.who.int.
2. Veeresha, P., Prakasha, D.G., Malagi, N.S., Baskonus, H.S., Gao, W.: New dynamical behaviour of the coronavirus (COVID-19) infection system with non local operator from reservoirs to people. Preprint march (2020).
3. Li, Q., et al.: Early transmission dynamics in Wuhan, China of novel Coronavirus-infected pneumonia. N. Engl. J. Med. **382**(13), 1199–1207 (2020)
4. Hu, B., Guo, H., Zhou, P., Shi, Z.L.: Characteristics of SARS-CoV-2 and COVID-19. Nat. Rev. Microbiol. **19**, 141–154 (2021)
5. Lu, H., Staratton, C.W., Tang, Y.W.: Outbreak of pneumonia of unknown etiology in Wuhan China: the mystery and the miracle. J Med Virol. **92**(04), 401–402 (2020)
6. Singhal, T.: A review of coronavirus disease-2019 (COVID-19). Indian J. Pediatr. **87**, 281–286 (2020)
7. Schlipkoter, U., Flahault, A.: Communicable diseases: achievements and challenges for public health. Public health Rev **32**(1), 90–119 (2010). https://doi.org/10.1007/BF03391594
8. Data collected from mohfw.gov.in.
9. Zheng, C., Zhang, W.: Real-world effectiveness of COVID-19 vaccines: a literature review and meta-analysis. Int. J. Infect. Dis. **114**, 252–260 (2022)
10. Turner, J.S., et al.: SARS-Cov-2 infection induces long-lived bone marrow plasma cells in humans. Nature (2021). https://doi.org/10.1038/s41586-021-03647-4
11. Feikin, D.R., et al.: Duration of effectiveness of vaccines against SARS-CoV-2 infection and COVID-19 disease: results of a systematic review and meta-regression. The Lancet (2022). https://doi.org/10.1016/S0140-6736(22)00152-0
12. Wang, Z., et al.: Naturally enhanced neutralising breadth against SARS-CoV-2 one year after infection. Nature (2021). https://doi.org/10.1038/s41586-021-03696-9
13. Nazeer, M., Hussain, F., et al.: Theoretical study of MHD electro-osmotically flow of third-grade fluid in micro channel. Appl. Math. Comput. **420**, 126868 (2022)
14. Chu, Y.-M., Shankaralingappa, B.M., et al.: Combined impact of Cattaneo-Christov double diffusion and radiative heat flux on bio-convective flow of Maxwell liquid configured by a stretched nano-material surface. Appl. Math. Comput. **419**, 126883 (2022)
15. Wang, J., Khan, M.I., et al.: Transportation of heat generation/absorption and radiative heat flux in homogeneous–heterogeneous catalytic reactions of non-Newtonian fluid (Oldroyd-B model). Comput. Methods Programs Biomed. **189**, 105310 (2020)
16. Zhao, T.-H., Khan, M.I., Chu, Y.-M.: Artificial neural networking (ANN) analysis for heat and entropy generation in flow of non-Newtonian fluid between two rotating disks. Math. Methods Appl. Sci. (2021). https://doi.org/10.1002/mma.7310
17. Hayat, T., Khan, S.A., Khan, M.I., Alsaedi, A.: Optimizing the theoretical analysis of entropy generation in the flow of second grade nanofluid. Phys. Scr. **94**, 085001 (2019)
18. Khan, M.I., et al.: Outcome for chemically reactive aspect in flow of tangent hyperbolic material. J. Mol. Liq. **230**, 143–151 (2017). https://doi.org/10.1016/j.molliq.2017.01.016
19. Hayat, T., et al.: Squeezing flow of second grade liquid subject to non-Fourier heat flux and heat generation/absorption. Colloid Polym. Sci. **295**(4), 967–975 (2017). https://doi.org/10.1007/s00396-017-4089-6
20. Qayyum, S., et al.: Comparative investigation of five nanoparticles in flow of viscous fluid with Joule heating and slip due to rotating disk. Phyica B Condens. Matter **534**, 173–183 (2018). https://doi.org/10.1016/j.physb.2018.01.044
21. Tomic, A., et al.: Divergent trajectories of antiviral memory after SARS-CoV-2 infection. Rs. Sq. (2021). https://doi.org/10.21203/RS.3.RS-612205/VI
22. Sheikh, N.A., et al.: Fractional model for MHD flow of Casson fluid with cadmium telluride nanoparticles using the generalized Fourier's law. Sci. Rep. **11**, 16117 (2021)
23. Ghanbari, B., Atangana, A.: A new application of fractional Atangana–Baleanu derivatives: Designing ABC- fractional masks in image processing. Phys A **542**, 123516 (2020)
24. Khan, M.A., et al.: Fractional investigations of zoonotic visceral leishmaniasis disease with singular and non-singular kernel. Eur. Phys J Plus **134**(10), 481 (2019)
25. Jan, R., Khan, M.A., et al.: Modeling the transmission of dengue infection through fractional derivatives. Chaos Solitons Fractals **127**, 189–216 (2019)
26. Zafer, Z.U.A., Ali, N., Baleanu, D.: Dynamics and numerical investigation of a fractional-order model of toxoplasmosis in the population of human and cats. Chaos, Soliton Fractals **151**, 111261 (2021)
27. Podlubny, I.: Fractional Differential Equations. Academic Press, San Diego CA (1999)
28. Owolabi, K.M., Atangana, A.: Numerical methods for fractional differentiation. Springer, Berlin (2019)

29. Ndolane, S.: Fractional advection-dispersion equation described by the Caputo left generalised fractional derivative. Palestine J. Math. **10**(2), 562–579 (2021)
30. Sweilam, N.H., Al-Mekhlafi, S.M., Assiri, T., et al.: Optimal control for cancer treatment mathematical model using Atangana–Baleanu–Caputo fractional derivative. Adv. Differ. Equ. **2020**, 334 (2020). https://doi.org/10.1186/s13662-020-02793-9
31. Atangana, A., Baleanu, D.: New fractional derivatives with nonlocal and non-singular kernel: theory and applications to heat transfer model. Therm. Sci. **20**(2), 763–769 (2016)
32. Raza, A., et al.: Natural convection flow of radiative maxwell fluid with Newtonian heating and slip effects: fractional derivatives simulations. Case stud. Therm. Eng. **28**, 101501 (2021)
33. Guo, B., Raza, A., et al.: Fractional-order simulations for heat and mass transfer analysis confined by elliptic inclined plate with slip effects: A comparative fractional analysis. Case Stud. Therm. Eng. **28**, 101359 (2021)
34. Atangan, A., Gomez-Aguilar, J.F.: Numerical approximation of Riemann–Liouville definition of fractional derivative: from Riemann–Liouville to Atangana–Baleanu. Numer Methods Part. Differ. Equ. **34**(5), 1502–1523 (2017)
35. Hasan, S., El-Ajou, A., Hadid, S., Al-Smadi, M., Momani, S.: Atangana Baleanu fractional framework of reproducing kernel technique in solving fractional population dynamics system. Chaos Solitons Fractals **133**, 1096249 (2020)
36. Momani, S., Arqub, O.A., Maayah, B.: Piecewise optimal fractional reproducing kernel solution and convergence analysis for the Atangana–Baleanu–Caputo model of The Lienard's equation. Fractals **28**(8), 2040007 (2020). https://doi.org/10.1142/S0218348X1
37. Momani, S., Maayah, B., Arqub, O.A.: The reproducing kernel algorithm for numerical solution of Van der pol damping model in view of the Atangana–Baleanu fractional approach. Fractals **28**(8), 2040010 (2020). https://doi.org/10.1142/S0218348X20400101
38. Arqub, O.A., Maayah, B.: Numerical solutions of integrodifferential equations of Fredholm operator type in the sense of the Atangana–Baleanu fractional operator. Chaos Solitons Fractals **117**, 117–124 (2018)
39. Arqub, O.A., Maayah, B.: Fitted fractional reproducing kernel algorithm for the numerical solutions of ABC—fractional Volterra integro-differential equations. Chaos Solitons Fractals **126**, 394–402 (2019)
40. Shiva, V.G.M., Reddy, K., Ranjith Kumar, G.: Non linear feedback control on Herd Behaviour Prey–Predator model affected by toxic substance. Int. J. Sci. Technol. Res. **9**(2), 5559–5564 (2020)
41. Vijayalakshmi, G.M.: Effect of herd behaviour prey-predator model with competition in predator. http://www.sciencedirect.com/science/article/pii/S2214785320327814.
42. Shah, K., Arfan, M., Mahariq, I., Ahmadian, A., Salahshour, S., Ferrara, M.: Fractal fractional Mathematical model addressing the situation of corona virus in Pakistan. Results Phys. **19**, 103560 (2020)
43. Oud, M.A., Ali, A., Alrabaiah, H., Ullah, S., Khan, M.A., Islam, S.: A fractional order mathematical model for COVID-19 dynamics with quarantine, isolation and environmental viral load. Adv. Differ. Equ. **2021**, 1–19 (2021)
44. Sinan, M., Shah, K., Kumam, P., Mahariq, I., Ansari, K.J., Ahmad, Z., Shah, Z.: Fractional order mathematical modelling of typhoid fever disease. Results Phys. **32**, 105044 (2022)
45. Shah, K., Abdeljawad, T., Mahariq, I., Jarad, F.: Qualitative analysis of a Mathematical model in the time of COVID-19. Biomed. Res. Int. **2020**, 5098598 (2020)
46. Abdo, M.S., Panchal, S.K., Shah, K., Abdeljawad, T.: Existence theory and numerical analysis of three species prey-predator model under Mittag Leffler power law. Adv. Differ. Equ. **2020**, 249 (2020)
47. Bushnaq, S., Shah, K., Alrabaiah, H.: On modelling of coronavirus-19 disease under Mittag–Leffler power law. Adv. Difference Equ. **2020**, 487 (2020)
48. Liu, X., et al.: Mathematical assessment of the dynamics of novel coronavirus infection with treatment: a fractional study. Chaos Solitons Fractals **153**, 111534 (2021)
49. Pata, V.: Fixed Point Theorems and Applications. Springer, Berlin (2019)
50. Debbouche. N, et al.: Chaotic dynamics in a novel COVID-19 pandemic model described by commensurate and incommensurate fractional –order derivatives. Non linear Dynamics (2021)
51. Dataset from ourworldindata.org, Recent updates of corona cases in India with vaccination count till end of October 2021.
52. Buşe, C., et al.: Hyer Ulam stability for linear differences with time dependent and periodic coefficients; the case when the monodromy matrix has simple eigen values. Symmetry **11**, 339 (2019)